Zao Cluster Workshop (24/Oct/2007)

Weak Lensing Analysis of Galaxy Clusters

Umetsu, Keiichi
(Academia Sinica IAA)

梅津敬一
（中央研究院天文所）

Contents

Lens Effects by a Galaxy Cluster

Images of background galaxies can be distorted coherently by the gravitational field of a foreground cluster:

Unlensed

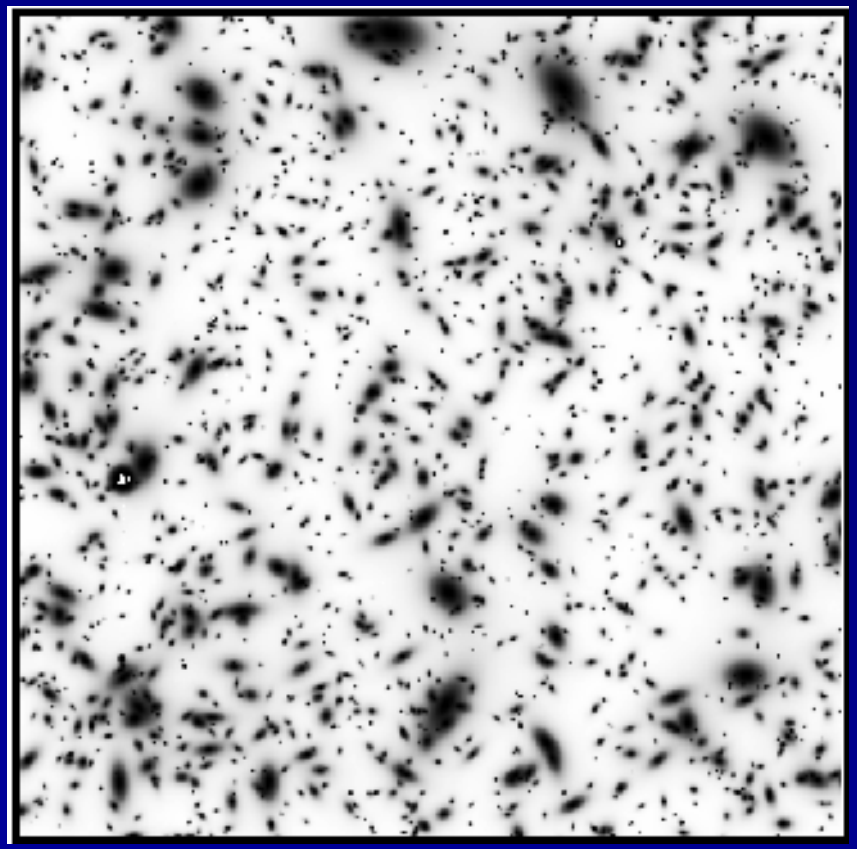

Lensed (simulated)

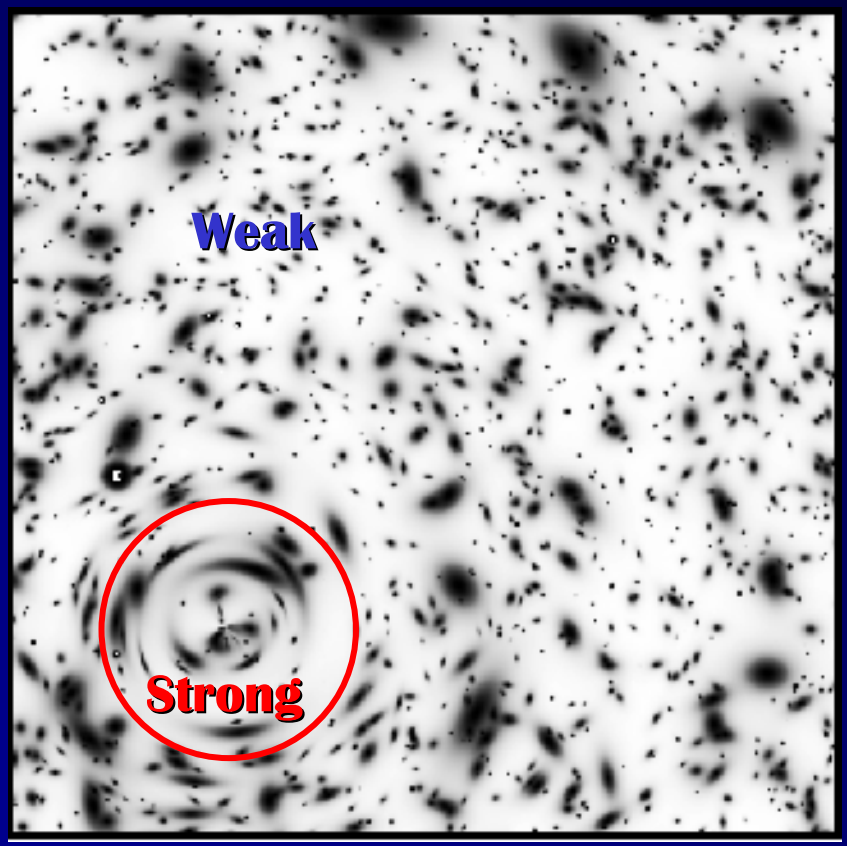

(Fort & Mellier)

Cluster Strong Lensing: Multiple Imaging

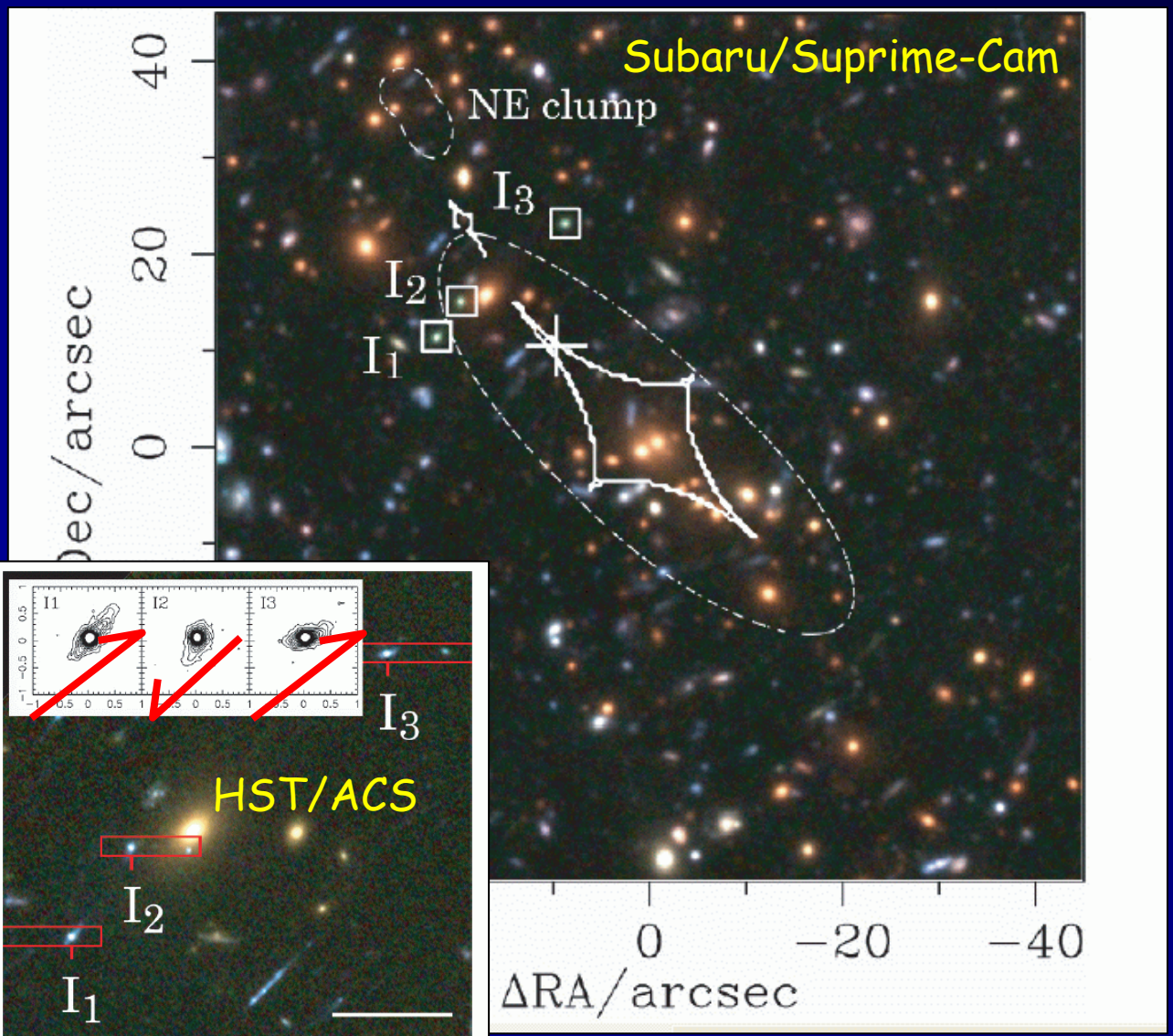

Lens: cluster at z=0.83

Source: galaxy at z=3.9 (t ~ 1.5Gyr)

Image positions and parities constrain the cluster mass distribution.

Umetsu, Tanaka, Kodama et al. 2005

“Special” Example of Cluster Weak Lensing

Weak Shearing = tangential shape distortion of background galaxy images

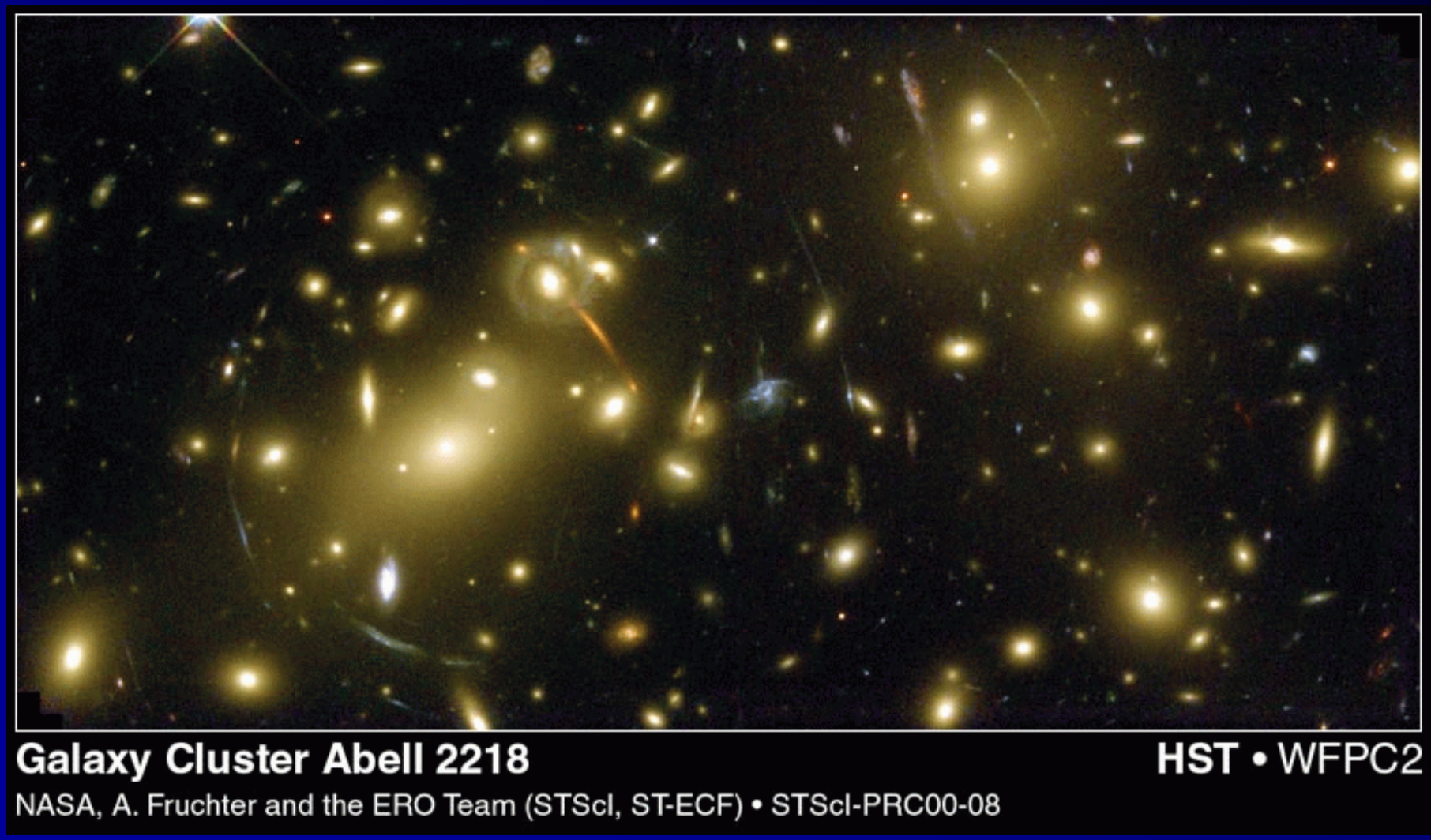

Weak Shear Field

Cluster z = 0.77; Arc z = 4.89:
Photo from H. Yee (HST/ACS)

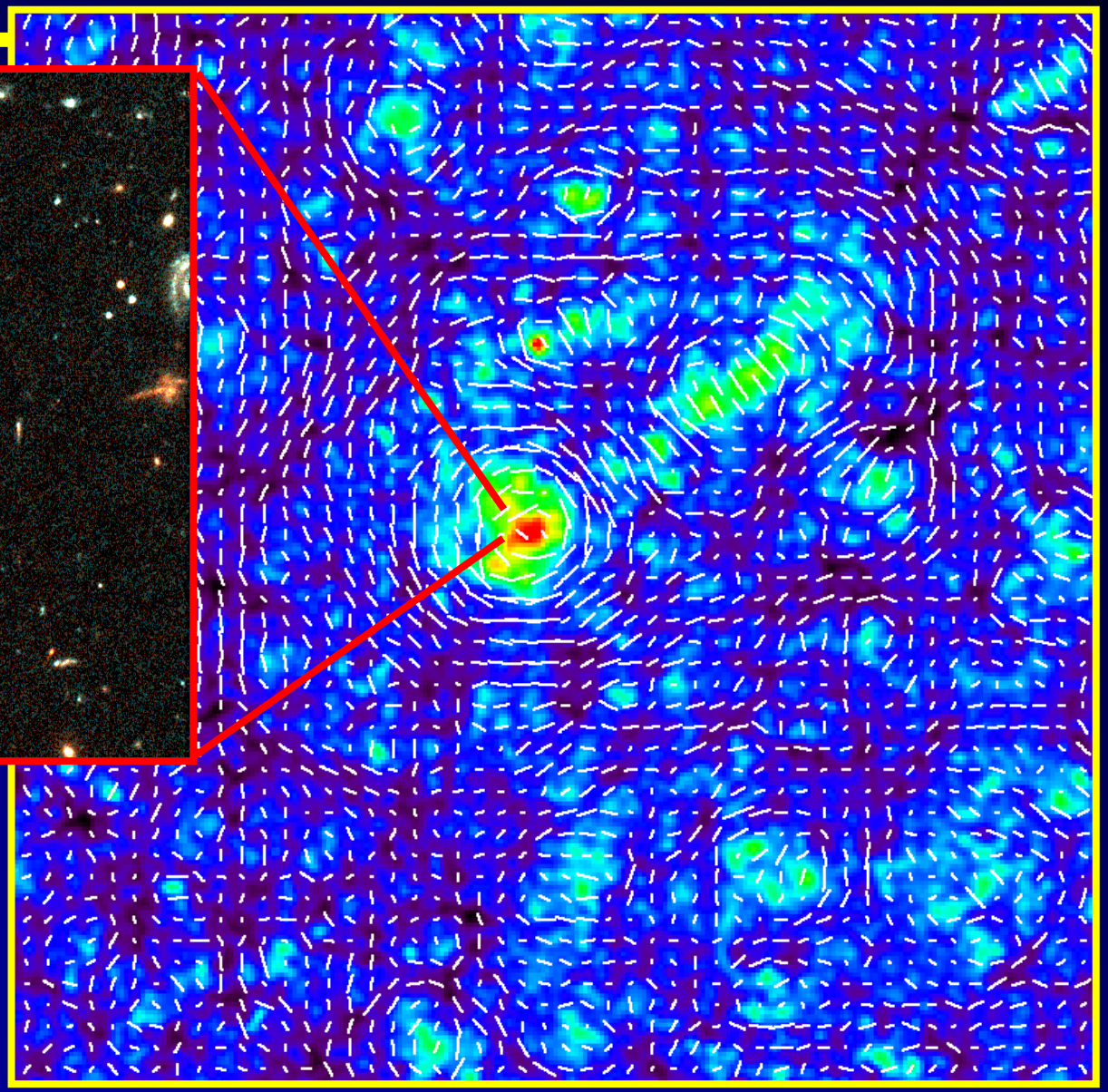

Simulated 3x3 degree field (Hamana 02)

1. Gravitational Lens Theory

1.1. Lens equation

1.2. Image distortion

1.3 Convergence & Shear

1.4 Strong to Weak Lensing Regimes

1.5 Geometric Scaling of Lensing Signal

References:

Bartelmann & Schneider (2001)

Ph.D. thesis of T. Hamana

Ph.D. thesis of M. Takada

Hattori, Kneib, & Makino (1999)

Umetsu, Tada, & Futamase (1999)

1.1. Gravitational Lensing

Gravitational deflection angle in the weak-field limit (|Φ|/c^2<<1)

$$\delta\hat{\alpha} \approx \frac{\delta p_{\perp}}{p_{\parallel}} = \frac{2}{c^2}\nabla_{\perp}\Phi(x_{\parallel}, x_{\perp})\delta x_{\parallel}$$

Lens equation

- weak field (|Φ|<<1), or small angle scattering (b>>2M) limit
- Born approximation

→ *simplify the various calculation*

$$\boldsymbol{\beta} = \boldsymbol{\theta} - \int_{\text{observer}}^{\text{source}} \frac{D_{ds}}{D_s} d\hat{\boldsymbol{\alpha}}$$

$$\equiv \boldsymbol{\theta} - \nabla\psi(\boldsymbol{\theta})$$

D: angular diameter distances

- Ds: observer to source
- Dd: observer to lens
- Dds: lens to source

Ψ: effective 2D lensing potential

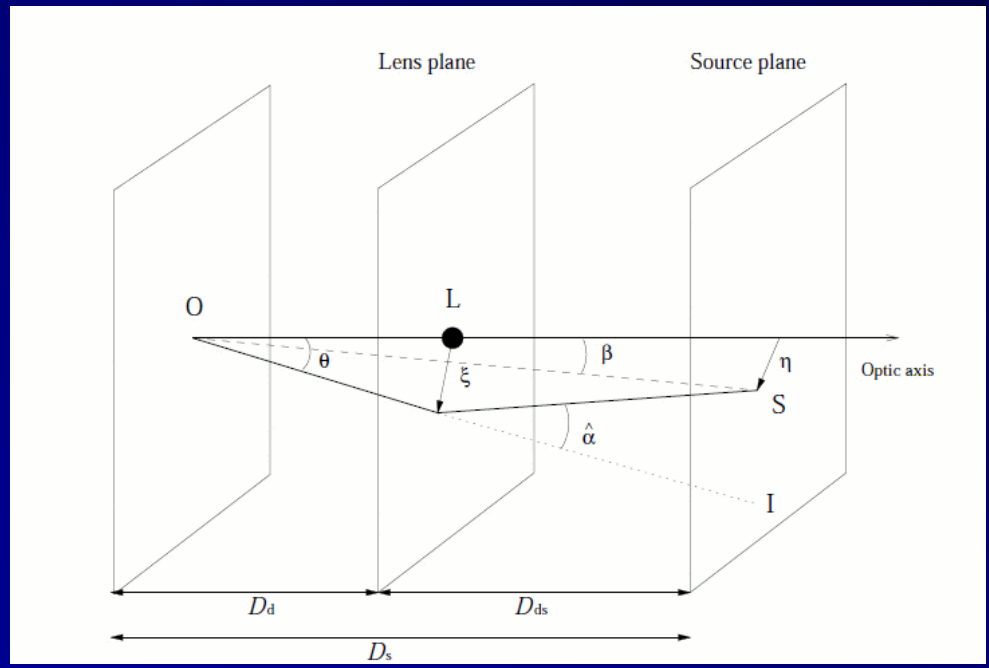

Cosmological Lens Equation

Solve the linearized geodesic eq. in the weak field limit (Futamase 95):

$$\boldsymbol{\theta}(\lambda_s) - \boldsymbol{\theta}(\lambda_o) = -\frac{2}{c^2}\int_{\text{null}} d\lambda \, \frac{r(\lambda_s - \lambda)}{r(\lambda_s)} \nabla_\perp \Phi(\lambda)$$

Functions defined with the affine parameter: $d\lambda = a\, d\chi$

Cosmological Poisson eq.:

$$(\Delta^{(3)} + 3K)\Phi(\boldsymbol{\chi}) = 4\pi G a^2 \left[\rho(\boldsymbol{\chi}) - \bar{\rho}\right]$$
$$\equiv 4\pi G a^2 \bar{\rho}\, \delta(\boldsymbol{\chi})$$

With Born approximation (Futamase 1995):

$$\boldsymbol{\beta} = \boldsymbol{\theta} - \frac{2}{c^2}\int_0^{\chi_s} d\chi_{//} \, \frac{r(\chi_s - \chi_{//})}{r(\chi_s)} \nabla_\perp \Phi(\boldsymbol{\chi}_\perp, \chi_{//})$$
$$= \boldsymbol{\theta} - \frac{2}{c^2}\int_0^{\chi_s} d\chi_{//} \, \frac{D_{ds}}{D_s} \nabla_\perp \Phi(\boldsymbol{\chi}_\perp, \chi_{//})$$

$\beta := \theta(\lambda s), \quad \theta := \theta(0)$

Functions defined with co-moving coordinates

…formally reduced to the conventional lens eq.

1.2. Image Distortion

Differential deflection causes a distortion in the "area" and "shape" of an image

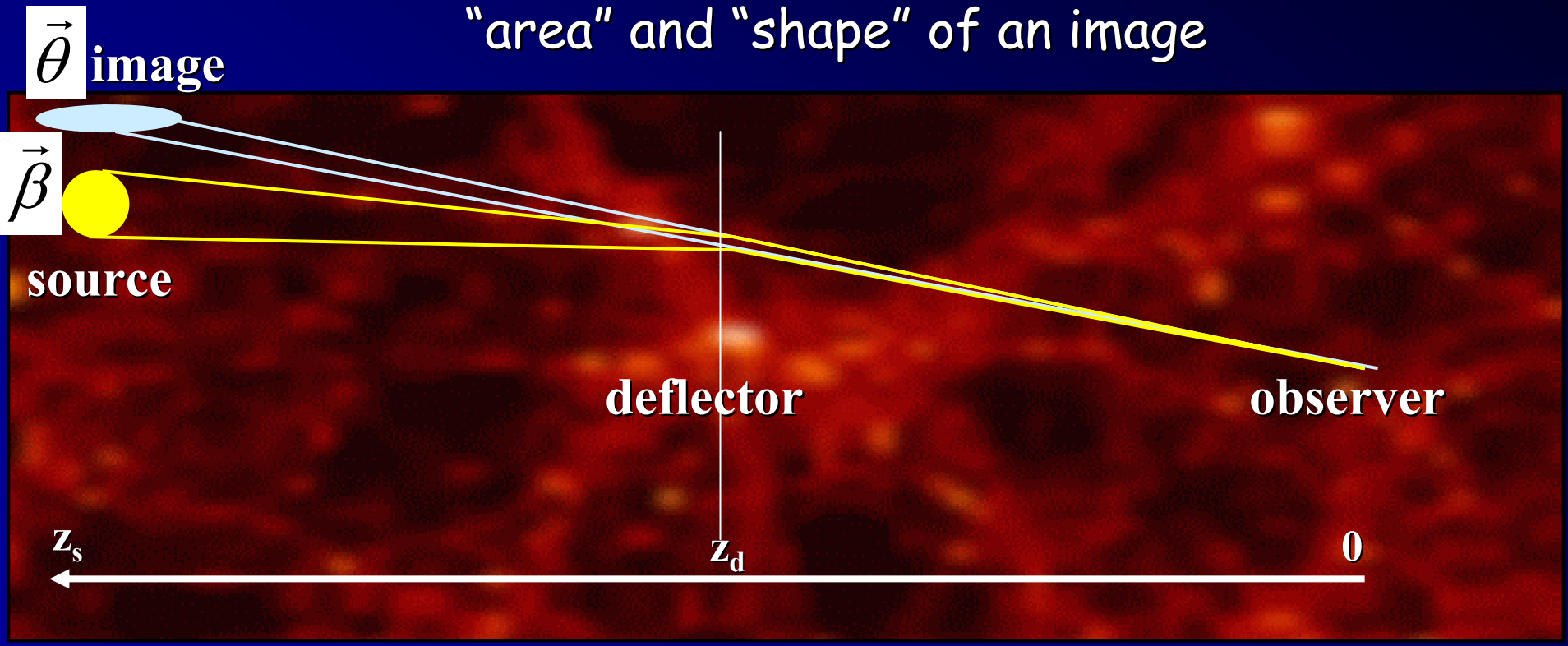

Deformation of the shape/area of an image

$$\delta\beta_i = D_{ij}^{(1)}\delta\theta_j + \frac{1}{2}D_{ijk}^{(2)}\delta\theta_j\delta\theta_k + \ldots$$

For an infinitesimal light source:

$$d^2\vec{\beta} = \mathbf{A}\, d^2\vec{\theta} \quad \text{with} \quad \mathbf{A} \equiv \mathbf{D}^{(1)} \neq \mathbf{1}$$

A: Jacobian matrix of the lens equation

1.3 Lensing Convergence and Shear

Symmetric 2x2 Distortion Matrix

described by 1+2 components

$$\mathbf{A}_{ij}(\boldsymbol{\theta}) = \delta_{ij} - \partial_i \partial_j \psi \equiv (1-\kappa)\delta_{ij} - \Gamma_{ij}$$

(1) Convergence κ

Isotropic area distortion, or flux magnification

(2) Gravitational shear matrix

Anisotropic quadruple (elliptical) shape distortion:

$$\kappa \equiv \frac{1}{2}\Delta\,\psi,$$

$$\Gamma_{ij} \equiv \left(\partial_i \partial_j - \frac{1}{2}\delta_{ij}\Delta_\theta\right)\psi = \begin{pmatrix} +\gamma_1 & \gamma_2 \\ \gamma_2 & -\gamma_1 \end{pmatrix}$$

Complex Shear: $\gamma = \gamma_1 + i\gamma_2$

2D effective potential,

as a L.o.S. projection of Newtonian potential

$$\psi(\boldsymbol{\theta}) = \frac{2}{c^2}\int_0^{\chi_s} \frac{d\lambda}{D_d}\frac{D_{ds}}{D_s}\Phi$$

Effect of Shear = Quadruple Distortion

Spin-2 Complex Shear

$$\gamma = \gamma_1 + i\gamma_2 \equiv |\gamma| e^{2i\phi_\gamma}$$

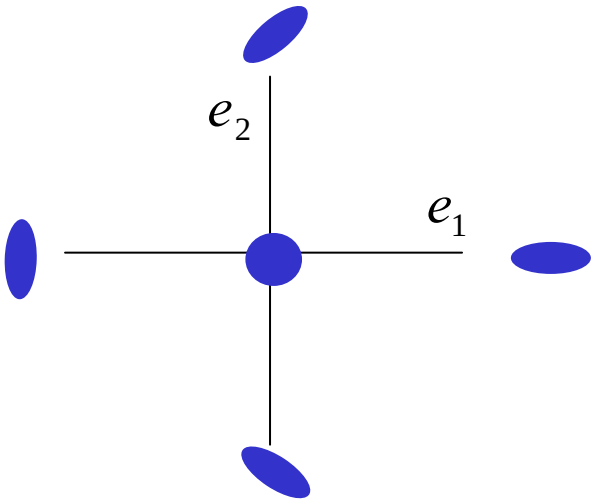

$$e = \frac{a^2 - b^2}{a^2 + b^2} e^{2i\phi} \Leftrightarrow Q + iU$$

Image quadrupoles:

$$Q_{ij} = \langle x_i x_j \rangle$$

Complex ellipticity, $e=e_1+ie_2$:

$$e_1 = \frac{Q_{11} - Q_{22}}{Q_{11} + Q_{22}}, \; e_2 = \frac{2Q_{12}}{Q_{11} + Q_{22}}$$

In the weak limit (κ,$|\gamma|$<<1):

$$e \approx e^{(s)} + 2\gamma$$

e(s): source intrinsic ellipticity

Assuming that background sources are statistically circular:

$$\langle e \rangle \approx 2\gamma + O\left(\frac{\sigma_e}{\sqrt{N}}\right)$$

Physical Meaning of κ

Lensing Convergence: weighted-projection of 3-D density contrast

$$\kappa = \frac{3H_0{}^2\Omega_m}{2c^2}\int_{\text{observer}}^{\text{source}} d\chi\; g(\chi,\chi_s)a^{-1}\frac{\delta\rho_m}{\bar{\rho}}$$

$$= \int d\lambda(\rho_{\text{m}} - \bar{\rho})\left(\frac{c^2}{4\pi G}\frac{D_s}{D_d D_{ds}}\right)^{-1} = \int d\Sigma_{\text{m}}\Sigma_{crit}{}^{-1}$$

Critical surface mass density of gravitational lensing

$$\Sigma_{\text{crit}}(z_d, z_s; \Omega_m, \Omega_{\text{DE}}, H_0) = \frac{c^2}{4\pi G}\frac{D_s}{D_d D_{ds}}$$

- **Strong lensing** $\kappa \sim 1$ @ high density regions (e.g., cluster cores)
- **Weak lensing** $\kappa < 1$ @ r = 100kpc – a few Mpc
- **Cosmic shear** $\kappa \sim 1\%$ @ large-scale structure (~10Mpc)

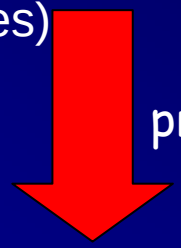

probability

1.4 Strong to Weak Lensing Regimes

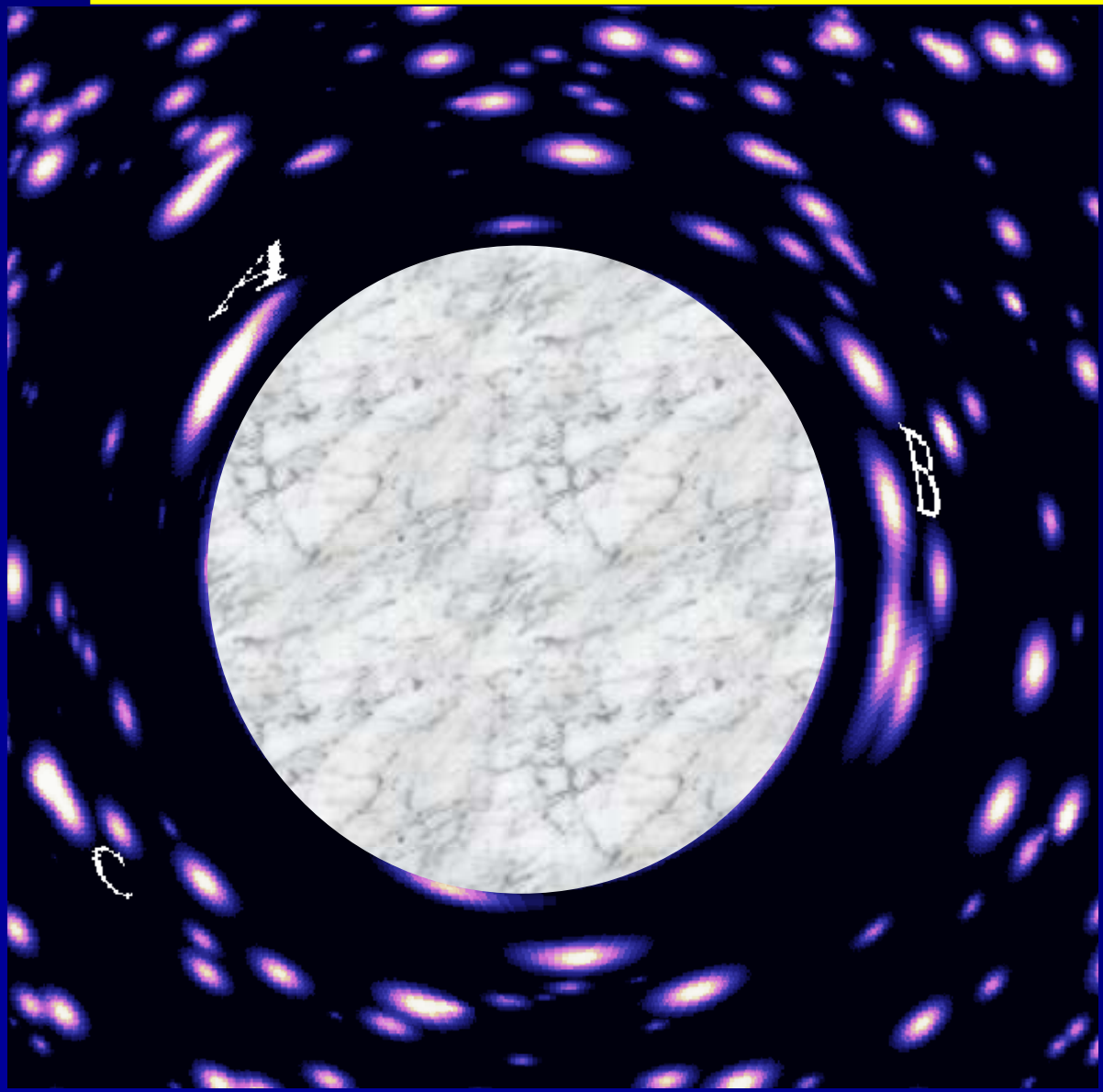

Tangential critical curve:

Einstein rings, Tangential arcs, Giant Luminous Arcs

$$\theta_{\mathrm{E}} = \left[\frac{4GM(\theta_{\mathrm{E}})}{c^2 D_d}\frac{D_{ds}}{D_s}\right]^{1/2}$$

$$\approx 20'' \left[\frac{M(\theta_{\mathrm{E}})}{10^{14} h^{-1} M_{\mathrm{sun}}}\right]^{1/2} \left(\frac{d_{ds}}{d_d d_s}\right)^{1/2}$$

Radial critical curve:

Radial arcs

SL: r <~ 0.5 arcmin

WL: r =~ 1' to 10'-20'

1.5 Geometric Scaling of Lensing Signal

$$g(a,a_s)=\frac{r(\chi,\chi_s)r(\chi)}{r(\chi_s)}=\frac{D_{ds}D_d}{D_s a}$$

g: geometric scaling function

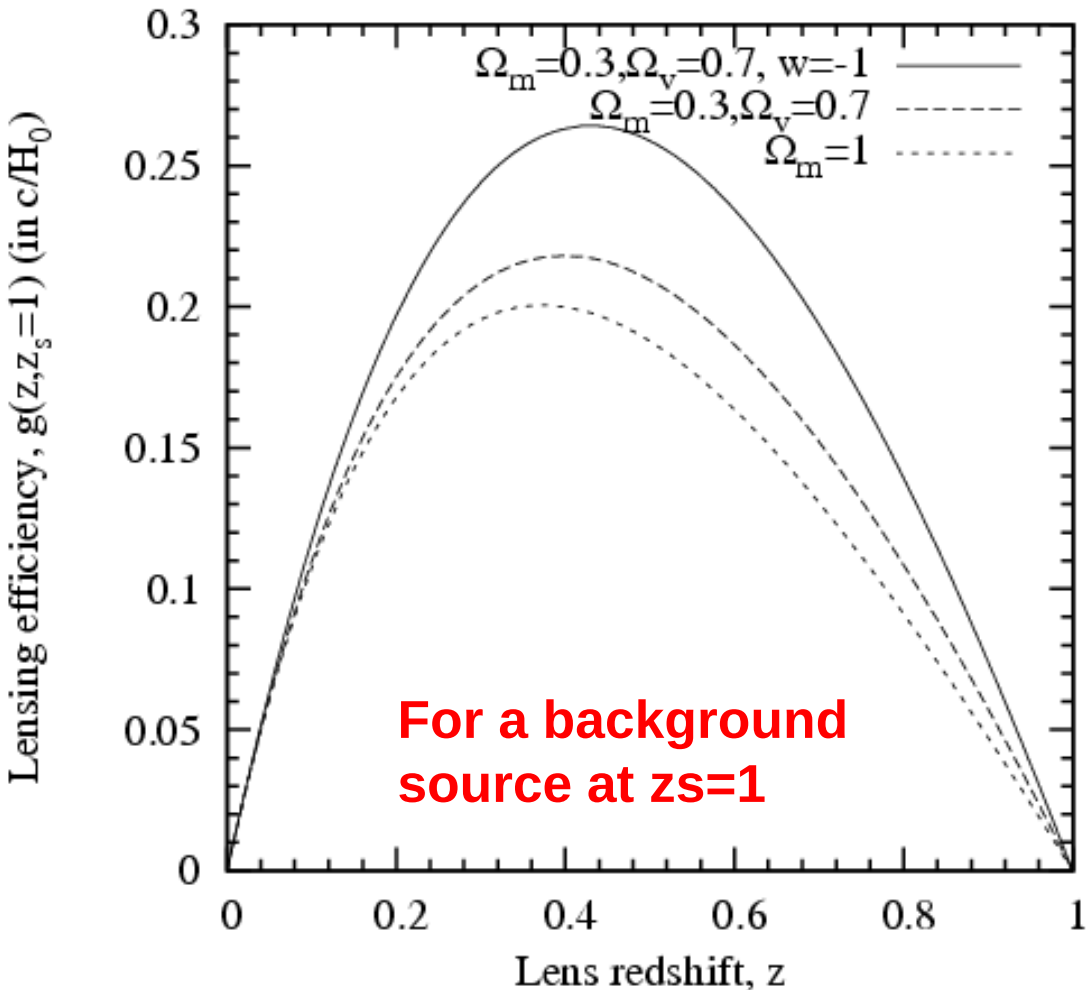

In optical observations, the median redshift of background galaxies is:

$$\langle z_s \rangle \approx 0.9\left(\frac{t_{\rm exp}}{30\,{\rm min}}\right)^{0.0667}$$

with the mean galaxy number density of

$$n_g \approx 40{\rm arcmin}^{-2}\left(\frac{t_{\rm exp}}{30\,{\rm min}}\right)^{0.3}\left(\frac{\rm FWHM}{0.8''}\right)^{-1}$$

(Hamana)

Systematic Uncertainties in Mass

Inverse critical density as a func of zd

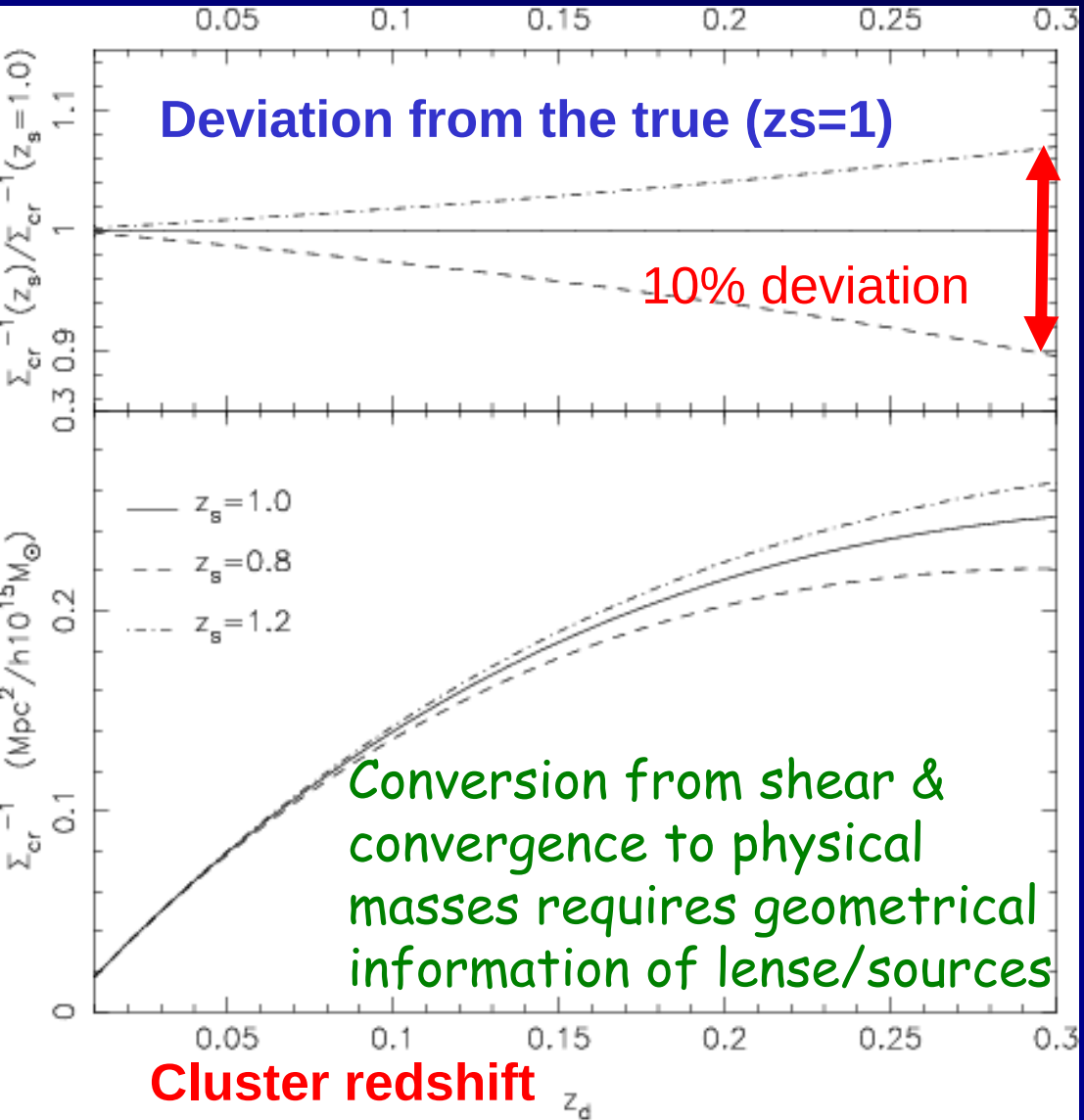

$$\text{Signal} \propto \Sigma_{crit}^{-1}(z_d, z_s) \propto D_d D_{ds} / D_s$$

In flat 3-space,

$$\text{Signal} \propto \chi_d (1 - \chi_d / \chi_s)$$

If $\chi_d << \chi_s$ (z_d <~ 0.2), the strength of gravitational lensing is insensitive to the source distance, i.e., no accurate information of redshift distribution is required.

Figure from Okabe & Umetsu (2007)

2. Cluster Weak Lensing

2.1 Weak Lensing E/B-mode Patterns

2.2 Tangential Shear Profile

2.3 Signal to Noise

2.4 Shear to Mass

2.5 Mass Reconstruction

2.1 E and B Mode Patterns

Formal similarities btw. shear and Stokes Q,U of linearly polarized light

Observable 2x2 shear tensor:

$$\Gamma_{ij} = \begin{bmatrix} +\gamma_1 & \gamma_2 \\ \gamma_2 & -\gamma_1 \end{bmatrix} \Leftrightarrow \begin{bmatrix} +Q & U \\ U & -Q \end{bmatrix}$$

Shear matrix in terms of potential:

$$\Gamma_{ij} = \left(\partial_i \partial_j - \frac{1}{2} \delta_{ij} \Delta \right) \psi_E + \frac{1}{2} \left(\varepsilon_{kj} \partial_i \partial_k + \varepsilon_{ki} \partial_j \partial_k \right) \psi_B$$

E,B-fields (rotation invariant) by projection of shear tensor

$$\begin{cases} \Delta\kappa_E = \partial_i \partial_j \Gamma_{ij} \Leftrightarrow E \\ \Delta\kappa_B = \varepsilon_{ij} \partial_i \partial_k \Gamma_{jk} \Leftrightarrow B \end{cases}$$

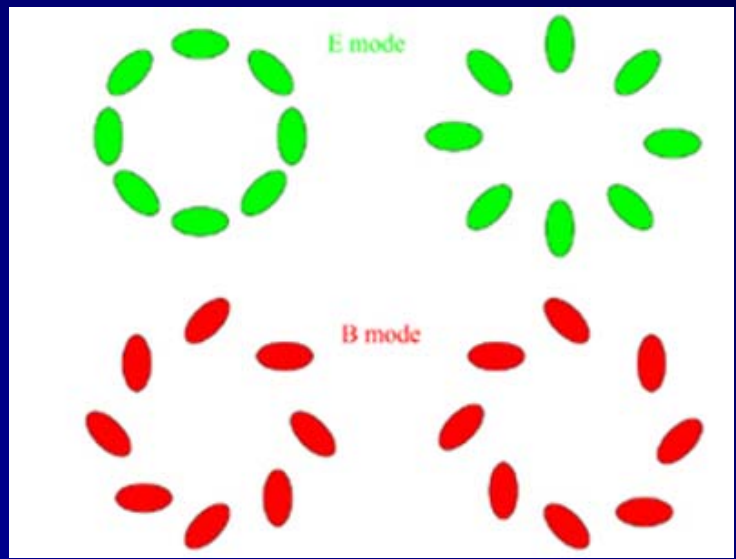

B-mode = 0 in Weak Lensing

➔ B-mode “signal” can be used to monitor systematics in shape measurements

2.2 Tangential Shear Profile

For a given point on the sky selected as a center, one can form a tangential (E-mode) projection of the spin-2 shear field:

$$\gamma_+ = -\left[\cos(2\phi)\gamma_1 + \sin(2\phi)\gamma_2\right]$$

Then, measure the azimuthally -averaged tangential shear profile as a function of angular radius

$$\langle\gamma_+(\theta)\rangle := \oint \frac{d\phi}{2\pi}\,\gamma_+(\boldsymbol{\theta})$$

This observable is related with differential information of "mass" properties:

$$\langle\gamma_+(\theta)\rangle = \bar{\kappa}(<\theta) - \langle\kappa(\theta)\rangle$$

mean κ within θ

$$\bar{\kappa}(<\theta) := \frac{2}{\theta^2}\int_0^\theta d\vartheta\,\vartheta\langle\kappa(\vartheta)\rangle$$

At large radii, $\kappa(r)\sim 0$, so that $\langle\gamma_+(\theta)\rangle \sim \bar{\kappa}(<\theta) \propto \frac{M(<\theta)}{\theta^2}$

Example: A1689 (Subaru/S-Cam)

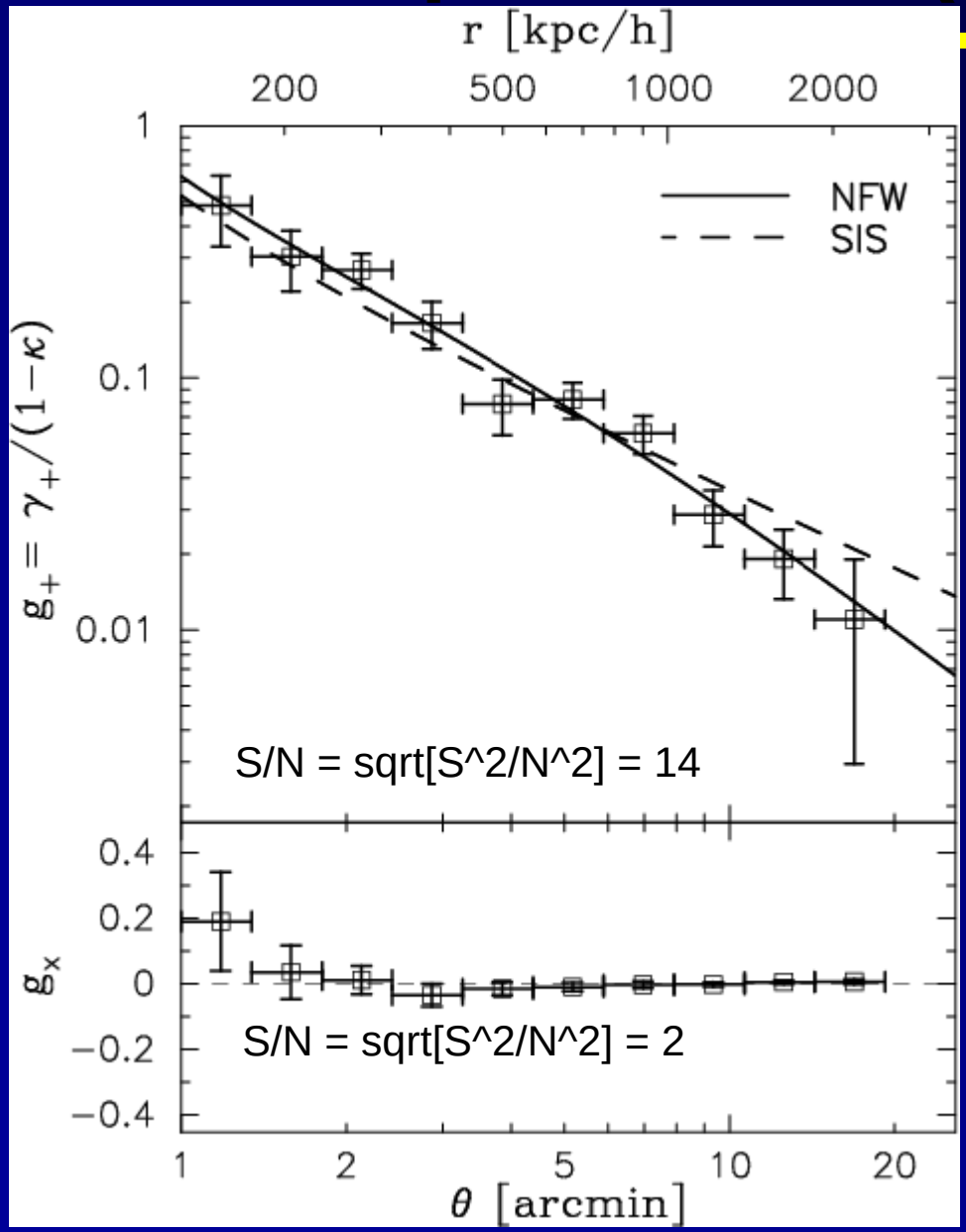

Tangential (E-mode) shear measurements (Top) from a red background sample, showing a significant coherent signal

B-mode shear measurements (Bottom), showing no significant systematics

- Measurements beyond the virial radius (~15')
- The errorbars are independent (no correlation)

V-i' selected red-galaxies (i'<25.5), n_g~10 arcmin^{-2}

2.3 S/N in Shear Estimates

Practical shear estimate:

$$\gamma_{\rm obs} = C\gamma + (\gamma_{\rm int} + \Delta\gamma_{\rm noise}) \qquad \langle \gamma_{\rm obs} \rangle = C\gamma$$

C: bias factor, need to be calibrated out

$\gamma_{\rm int}$: intrinsic ellipticity

$\Delta\gamma_{\rm noise}$: shape measurement error

Now assume C=1 (no systematic bias, or perfect calibration):

$$\sigma_g = \sqrt{\sigma_{\rm int}^{\ 2} + \sigma_{\rm noise}^{\ 2}} \approx 0.3 - 0.4$$

from Subaru/S-Cam observations

S/N of amplitude of averaged shear in a pixel from a local sample of N-galaxies

$$\mathrm{S/N}_{|\gamma|} = \left| \gamma \right| \Big/ \left(\sigma_g / \sqrt{N} \right) \approx 2.4 \left(\frac{|\gamma|}{0.1} \right) \left(\frac{\sigma_g}{0.4} \right)^{-1} \left(\frac{n_g}{30\mathrm{arcmin}^{-2}} \right)^{1/2} \left(\frac{\Delta\theta}{1'} \right)$$

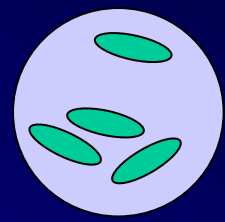

S/N of azimuthally averaged tangential shear for an SIS halo

$$\mathrm{S/N}_{\gamma+} \sim \left(\gamma_+ \Big/ \sigma_g / \sqrt{2N} \right) \approx 12 \left(\frac{\sigma_v}{1000\mathrm{km/s}} \right)^2 \left(\frac{\sigma_g}{0.4} \right)^{-1} \left(\frac{n_g}{30\mathrm{arcmin}^{-2}} \right)^{1/2} \left(\frac{\ln(\theta_{\max}/\theta_{\min})}{\ln 10} \right)^{1/2} \left(\frac{\langle D_{ds}/D_s \rangle}{0.7} \right)$$

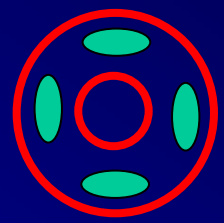

S/N in Mass Maps

Sensitivity in the reconstructed mass map is:

$$\sigma_\kappa = \frac{\sigma_g}{\sqrt{2N}} = 0.034\left(\frac{\sigma_g}{0.4}\right)\left(\frac{\mathrm{FWHM}}{1'}\right)^{-1}\left(\frac{n_g}{30\mathrm{arcmin}^{-2}}\right)^{1/2}$$

FWHM: Gaussian FWHM in the mapmaking

To have an S/N of, say, $\nu := \kappa/\sigma_\kappa = 5$, for an unresolved mass halo with $\kappa = 0.2$,

$$\mathrm{FWHM} = 0.85''\left(\frac{\nu}{5}\right)\left(\frac{\kappa}{0.2}\right)^{-1}\left(\frac{\sigma_g}{0.4}\right)^{-1}\left(\frac{n_g}{30\mathrm{arcmin}^{-2}}\right)^{1/2}$$

In weak lensing mapmaking from ground-based observations, the effective angular resolution is of the order of 1 arcmin

To resolve substructures,

(1) Study nearby clusters (Okabe & Umetsu 2007, to appear in PASJ)

(2) Go to space (HST)

(3) Use weak lensing Flexion (Okura,Umetsu,Futamase 2007ab)

2.4 Shear to Mass

Observable shear (image ellipticity) field to a mass map

$$\partial_i \kappa = \partial^j \Gamma_{ij} \equiv (\vec{u}_\gamma)^i$$

$$\kappa = \Delta^{-1}\left(\partial^i \partial^j \Gamma_{ij}\right) = \Delta^{-1}\left(\vec{\nabla} \cdot \vec{u}_\gamma\right)$$

Solve the integral eq from measured shear field for a given survey geometry (boundary condition + constant mass sheet)…

Kaiser & Squires 1993

$$\hat{\kappa}(\vec{l}) = \cos(2\phi_l)\,\hat{\gamma}_1(\vec{l}) + \sin(2\phi_l)\,\hat{\gamma}_2(\vec{l}), \quad \vec{l} \neq 0$$

Uses the Green function for the 2D Poisson equation to solve the inversion equation; usually, l=0 mode is taken to be zero

On large scales (>10 Mpc), $\langle \delta_{matter} \rangle = 0$.

→ Justification of using Kaiser & Squires method with $\langle \kappa \rangle = 0$

Weak Shear Map – E-mode Pattern

Cluster z = 0.77; Arc z = 4.89:
Photo from H. Yee (HST/ACS)

WL Cluster Survey
(Hamana-san's talk):

Schneider 96, Hamana et al. 2004;

Umetsu & Futamase 2000, Miyazaki et al. 2002

Simulated 3x3 degree field (Hamana 02)

3. Weak Lensing Analysis

3.1 Practical Approaches: KSB, Shapelets

3.2 Observable Image Ellipticity

3.3 Star/Galaxy Separation

3.4 PSF Corrections

3.5 Weak Lensing Dilution Effect

References:

Kaiser, Squires, Broadhurst (KSB 1995)

Erben et al. (2001)

Hoekstra et al. (1998)

Bartelmann & Schneider (2001)

Refregier (2003)

Shear Testing Programme (STEP)

3.1 Practical Approaches

Practical observations suffer from:

- Noise in shape measurements of faint, small distant galaxies
- PSF anisotropy (5-10%) varying from position to position
- Smearing of the lensing signal due to atmospheric smearing

How to improve the shape measurement?

How to correct for the PSF effects?

How to obtain the unbiased shear estimate?

- **KSB method based on the moment approach** (KSB95)

Quantify the shapes of images by Gaussian-weighted quadrupole shape moments

IMCAT :: KSB-implementation for object detection, shape measurements

KSB (1995) made Weak Lensing a reliable observational tool!!!

- **Shapelets** based on a complete, orthonormal set of 2D basis functions constructed from **Hermite** polynomials weighted by a **Gaussian** (Refregier 2003)

3.2 Observable Image Ellipticity

Observable ellipticity is expressed as a linear sum of (1) intrinsic, (2) gravitational shear, (3) PSF contributions in the limit of "weak" shearing both in lensing and PSF (KSB 1995, Bartelmann & Schneider 2001):

Ellipticity measured for a background galaxy

$$e_\alpha = e_\alpha^{(s)} + P_{\alpha\beta}^{\gamma}\gamma_\beta + P_{\alpha\beta}^{sm}q_\beta$$

e^(s): intrinsic ellipticity of the background

q: quadrupole PSF anisotropy (CCD, stacking error etc.)

P^γ: response for gravitational shearing

P^sm: response for PSF anisotropy

Ellipticity for a foreground star

$$e_\alpha^* = P_{\alpha\beta}^{sm*}q_\beta$$

since e^(s)=γ=0

3.3 Star/Galaxy Separation

Sample of foreground + cluster + background galaxies

Sample of bright, unsaturated stars (a few stars per arcmin^2) for measuring PSF size/shape properties

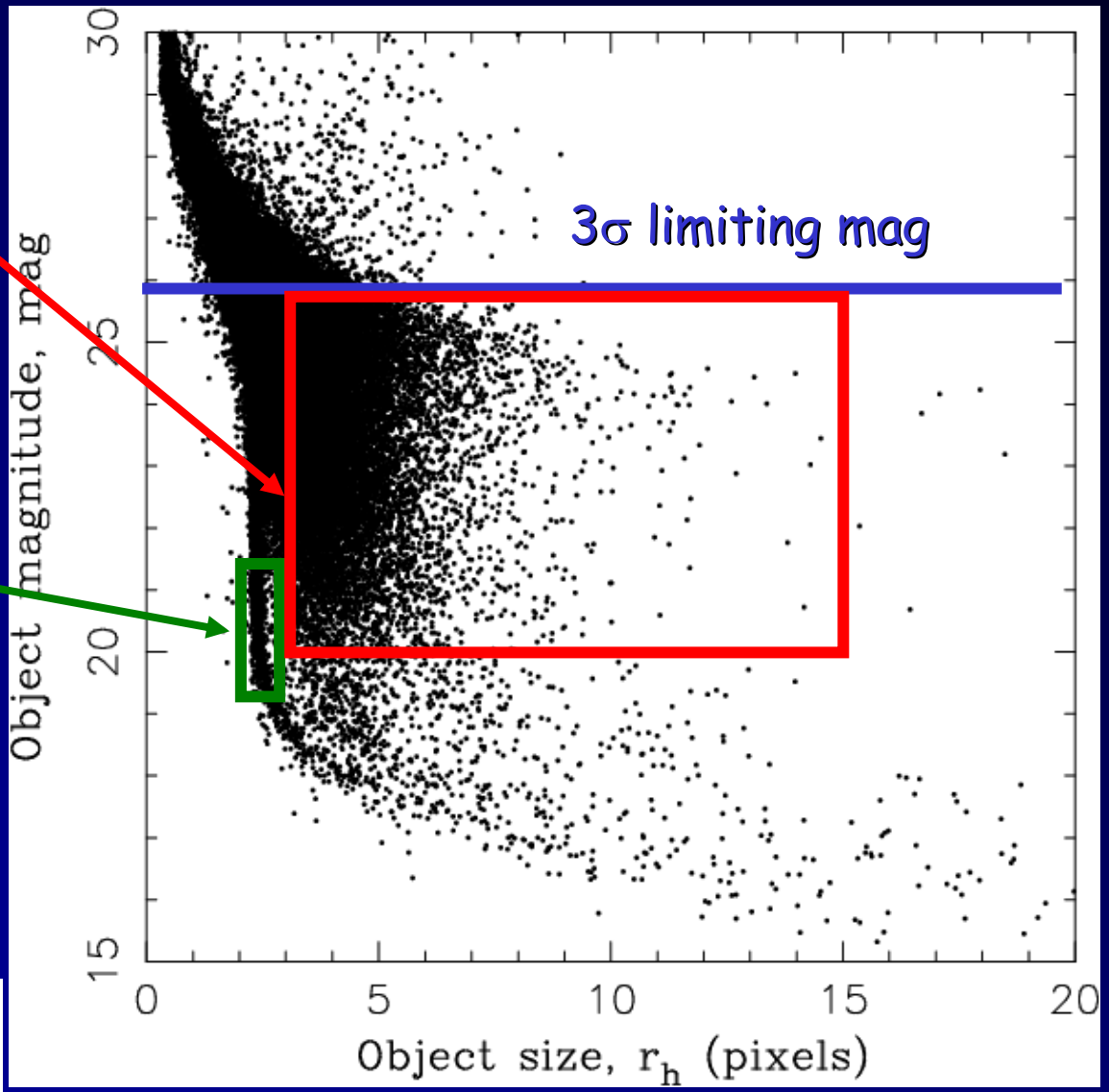

A1689 field (Subaru/S-Cam)

cf. number of usable field galaxies in S-Cam data (Hamana)

$$n_g \approx 40\,\mathrm{arcmin}^{-2}\left(\frac{t_{\mathrm{exp}}}{30\,\mathrm{min}}\right)^{0.3}\left(\frac{\mathrm{FWHM}}{0.8''}\right)^{-1}$$

3.4 PSF Anisotropy Correction

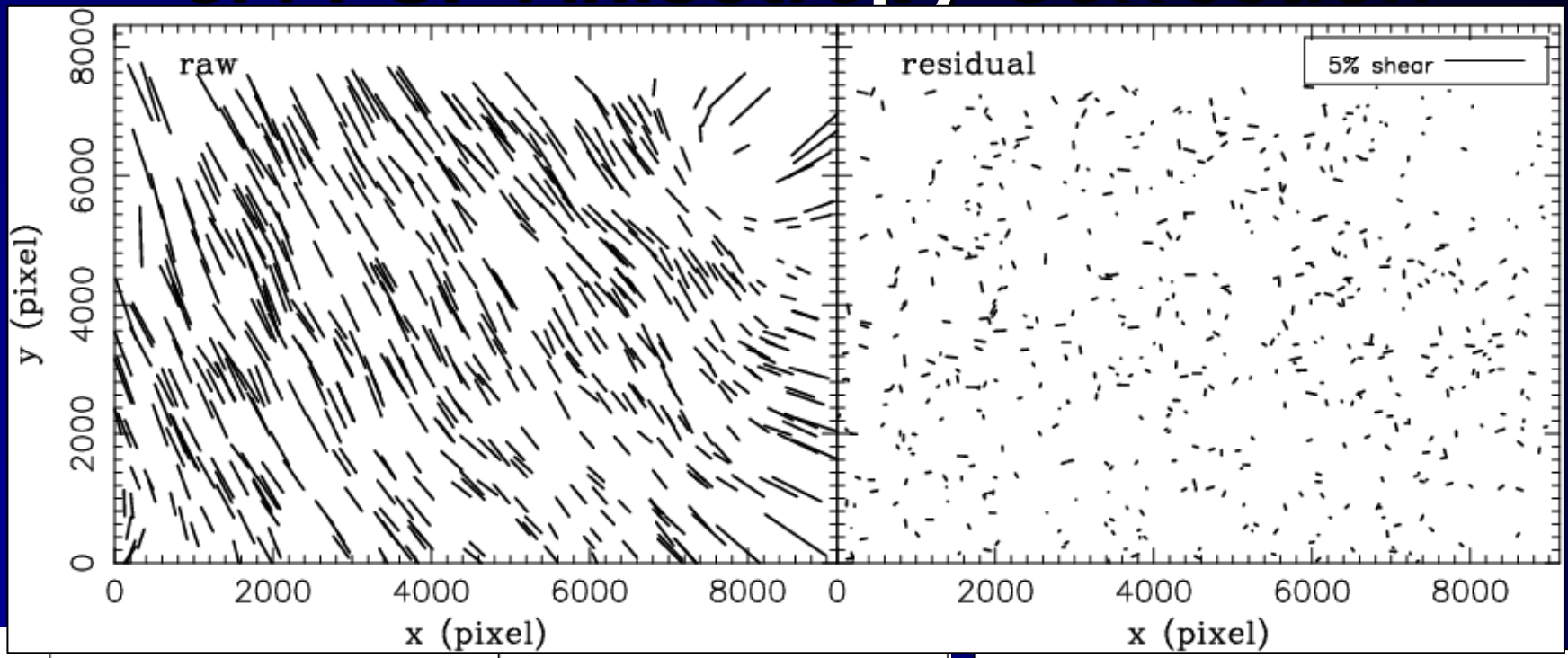

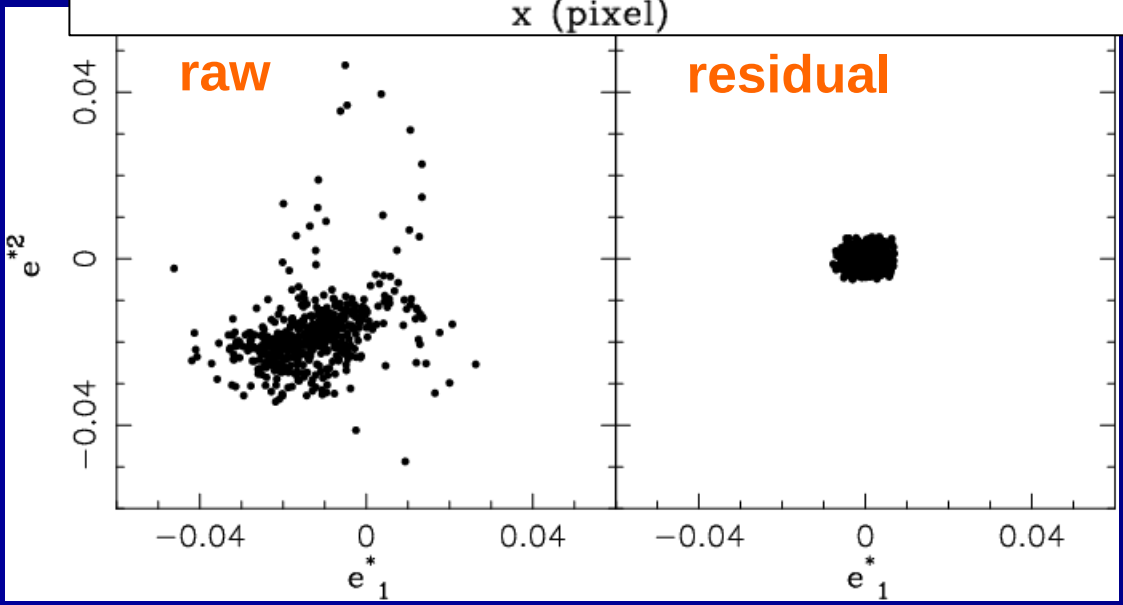

$$e^*_\alpha = P^{sm*}_{\alpha\beta} q_\beta$$

Subaru/S-Cam data of A1689 (i'-band)

Seeing FWHM=0.8"

Isotropic Shear Calibration

Mean shear calibration factor, as a function of object size

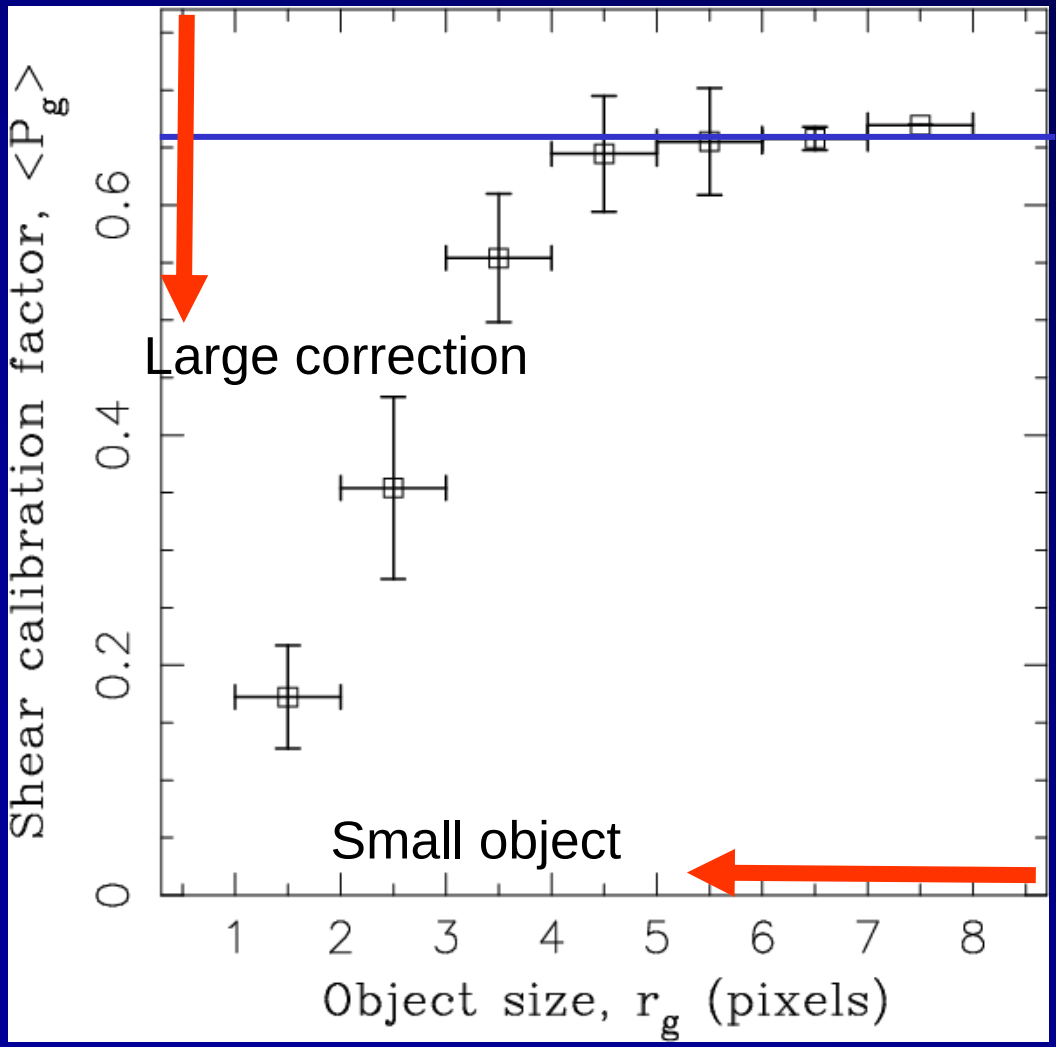

Anisotropy correction for individual galaxy ellipticities:

$$e' = e - P^{sm} q$$

Isotropic correction:

$$\gamma \approx P_\gamma^{-1} e'$$

Small objects are more affected by atmospheric smearing

1pixel = 0.202 arcsec (S-Cam)

3.5 Weak Lensing Dilution Effect

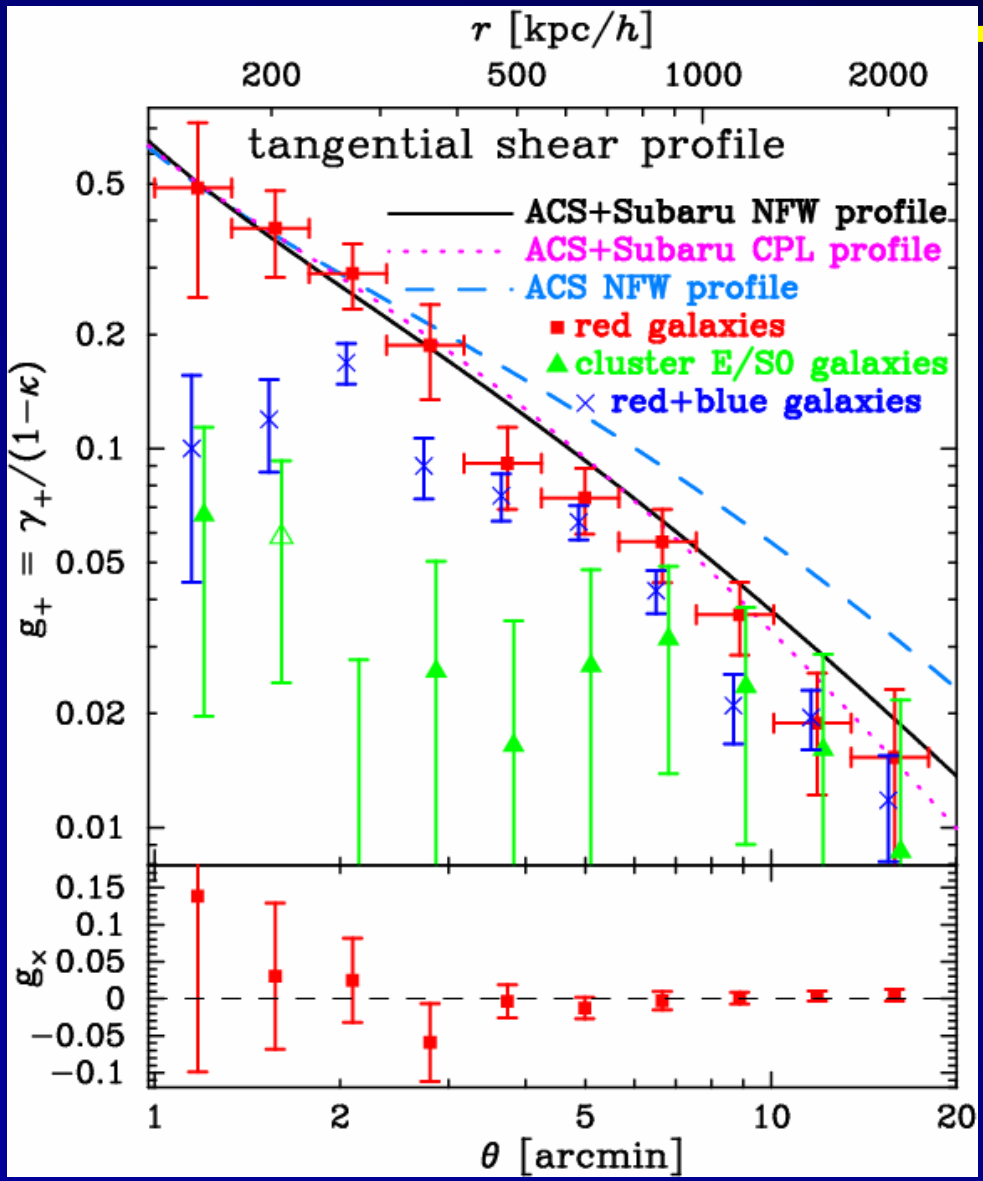

Broadhurst, Takada, Umetsu et al. (2005)

Averaged shear over a local sample of "Background" + "Cluster" galaxies:

$$\langle \gamma_{diluted} \rangle = \langle \gamma_{BG} \rangle \frac{N_{\rm BG}}{N_{\rm BG} + N_{\rm Cluster}}$$

Dilution factor:

$$1 + f_{dilution} \equiv 1 + \frac{N_{\rm cluster}}{N_{\rm BG}}$$

In the central region of a rich cluster, the degree of dilution is as large as f~4!!

A secure background selection is crucial!!

Background Color Selection

Color-Magnitude Diagram for A1689 (z=0.183)

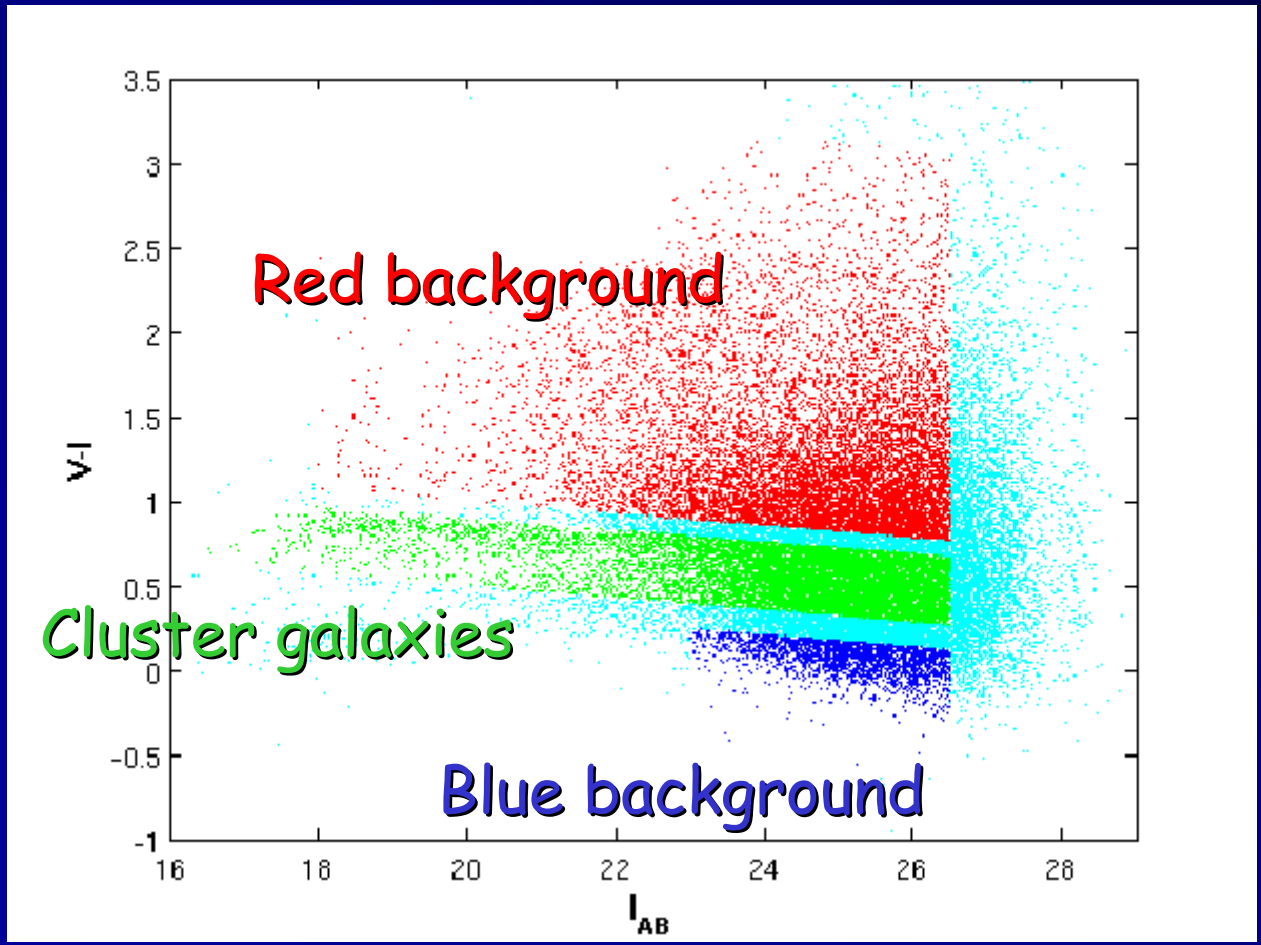

Red sample

<zs>=0.87,
$<D_{ds}/D_s>$=0.69

Faint blue sample

<zs>=2.0

$<D_{ds}/D_s>$=0.83

After color-selection, n_g(red) ~ 5-10 galaxies / arcmin^2 in z=0.1-0.2 clusters

Medezinski, Broadhurst, Umetsu et al. (2007)

4. Weak Lensing Observations

4.1 1D Mass Profile Reconstruction of A1689

4.2 2D Mass Reconstruction of Clusters

4.1 1D Mass Reconstruction (A1689)

Wide-field imaging of Subaru/Suprime-Cam

Broadhurst, Takada, Umetsu et al. 2005

Revealing ~100 lensed multiple images of ~30 background galaxies

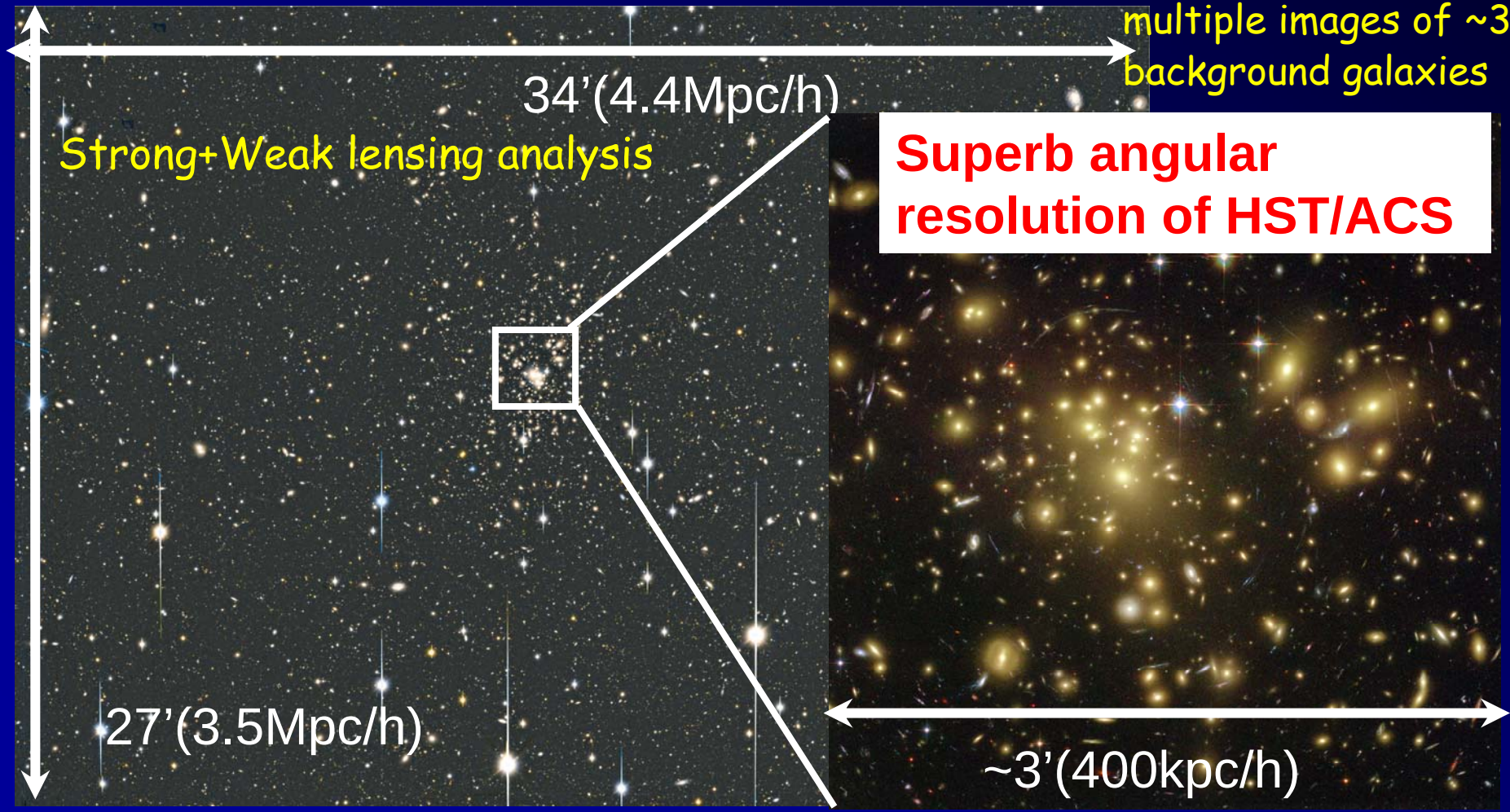

Superb angular resolution of HST/ACS

Weak Shearing + Magbias Measurements combined with ACS Strong Lensing

- Combines 1D **Weak** (1) **shear** and (2) **magnification bias** measurements to derive a model-independent, mass density profile, $\kappa(\theta)$
  - Distortion alone ➔ mass-sheet degeneracy (no constraint on l=0)
  - Magnification bias ➔ breaking the degeneracy (noisier in general)
- Then, combines **Strong** and **Weak Lensing** mass profiles $\kappa(\theta)$ to test the CDM / NFW model over 10<r<2000 kpc/h (!!)

Magnification Bias

$$\delta n / n_0 \approx 2(\alpha - 1)\kappa, \quad \alpha < 1$$

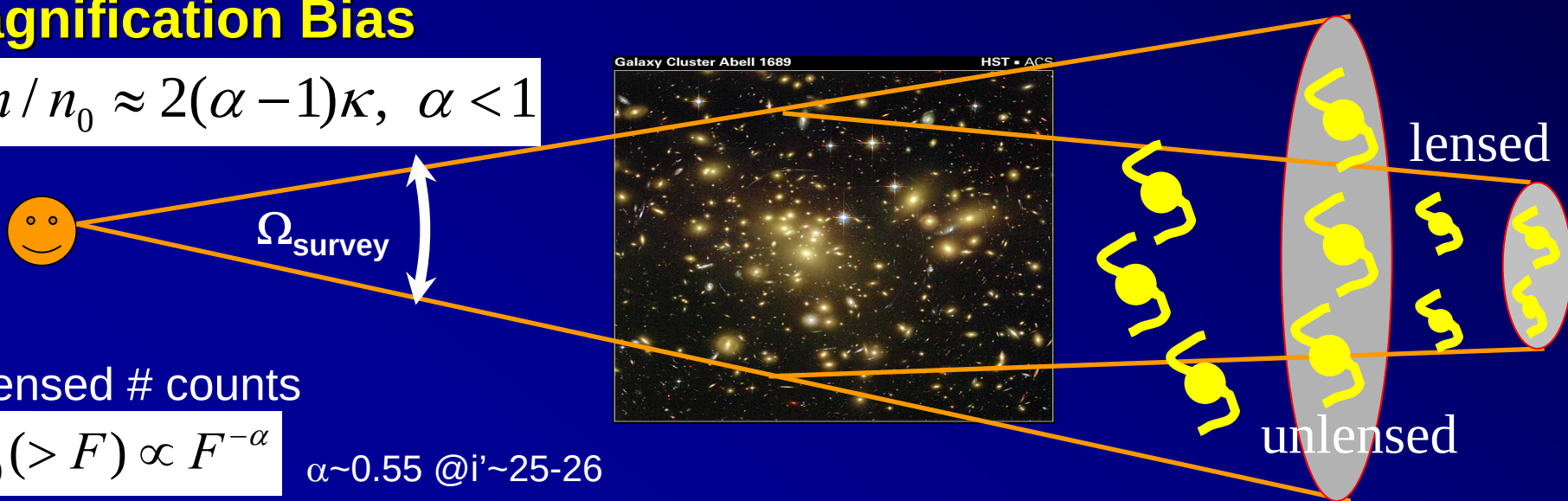

unlensed # counts

$$n_0(>F) \propto F^{-\alpha}$$

α~0.55 @i'~25-26

Mass profile @ $0.005r_{vir}$ to r_{vir}

Projected mass density profile

22 data points used

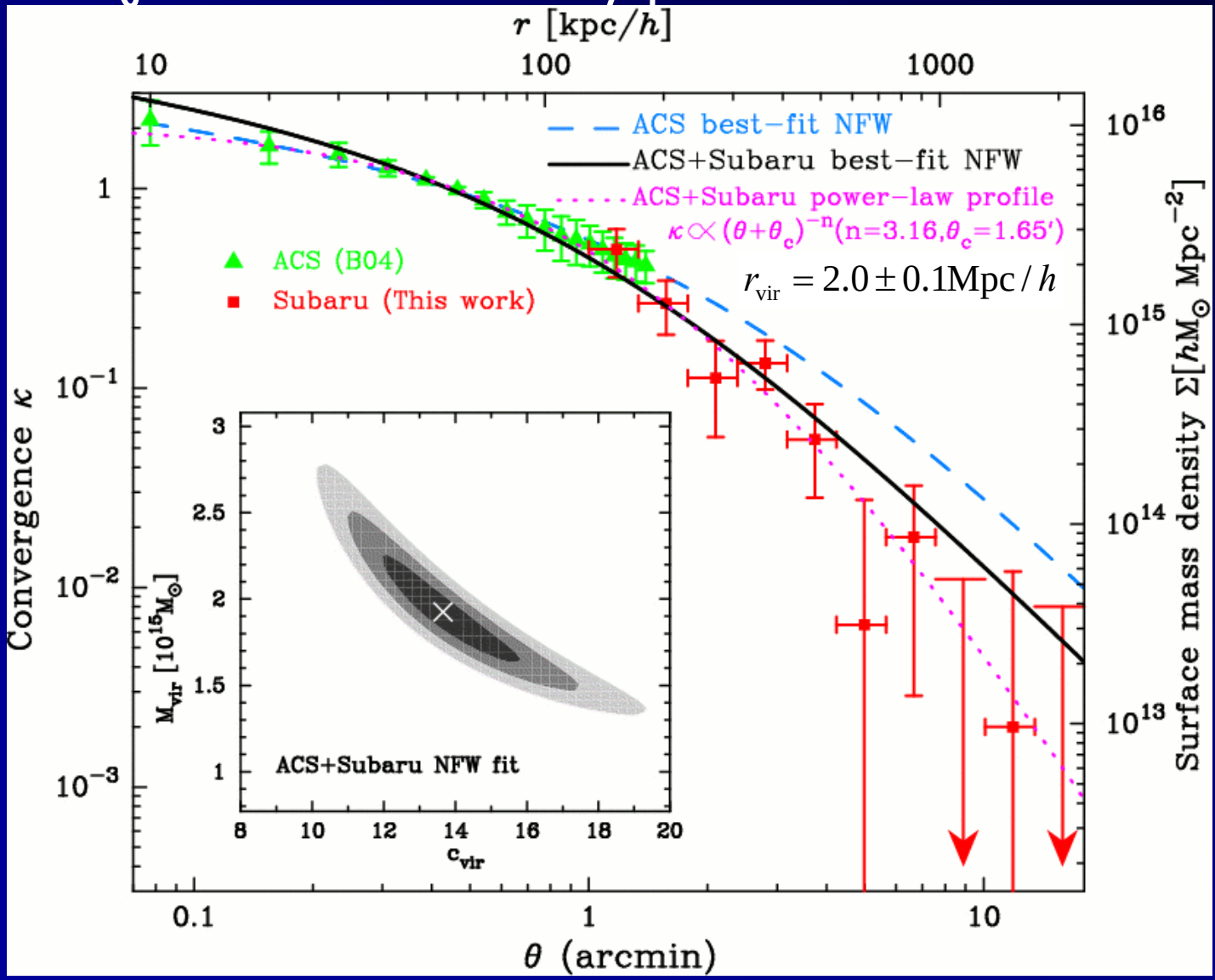

- CDM acceptable

$\chi^2_{\rm min}/{\rm dof.} = 13./20$

$M_{\rm vir} = 1.93^{+0.2}_{-0.2} \times 10^{15} M_{\rm sun}$

$c_{\rm vir} = 13.7^{+1.4}_{-1.1}$

- Cored Pow-Law preferred

$\chi^2_{\rm min}/{\rm dof.} = 4.5/19$

$n = 3.16^{+0.81}_{-0.72}$

$r_c = 214^{+99}_{-78}\,{\rm kpc}/h$

- SIS/Cored-IS

Strongly rejected (>10σ!!)

4.2 2D Mass Reconstructions

Gravitational shear field

Magnification bias measurement

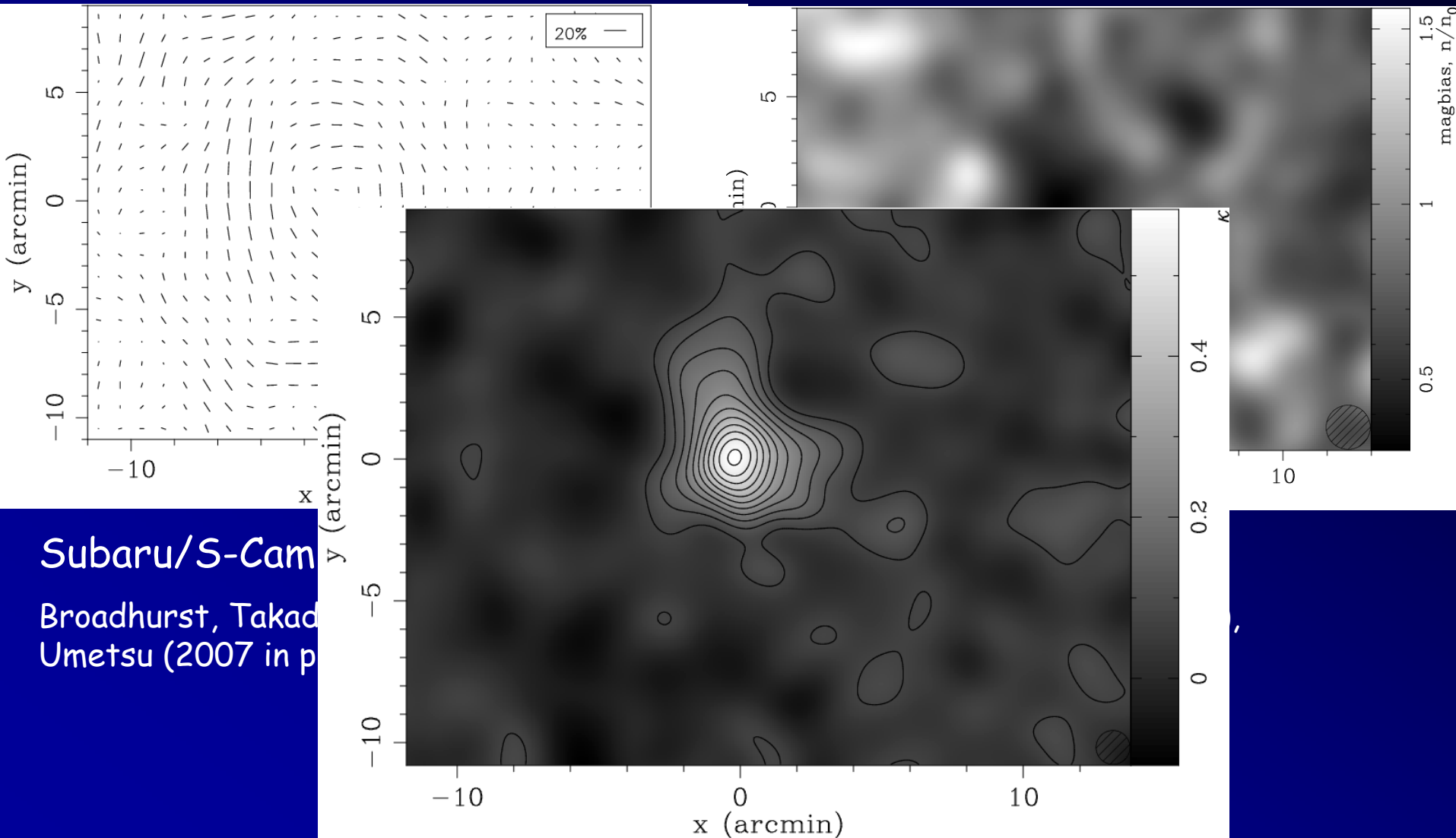

Subaru/S-Cam

Broadhurst, Takad

Umetsu (2007 in p

Mass and Light in A1689

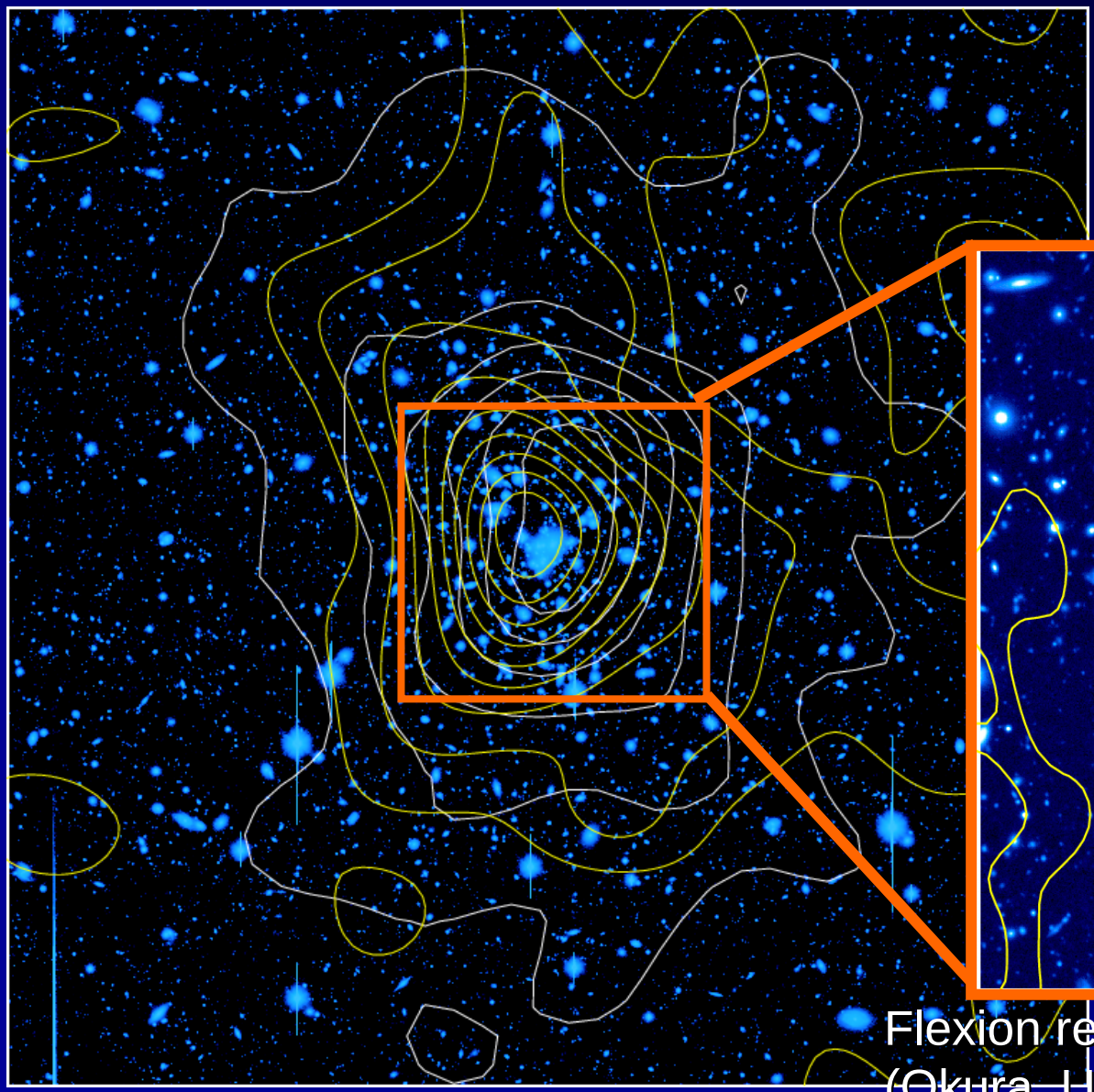

Subaru i'-image + Mass (yellow) + Light (white) contours in the central 15'x15' region of A1689

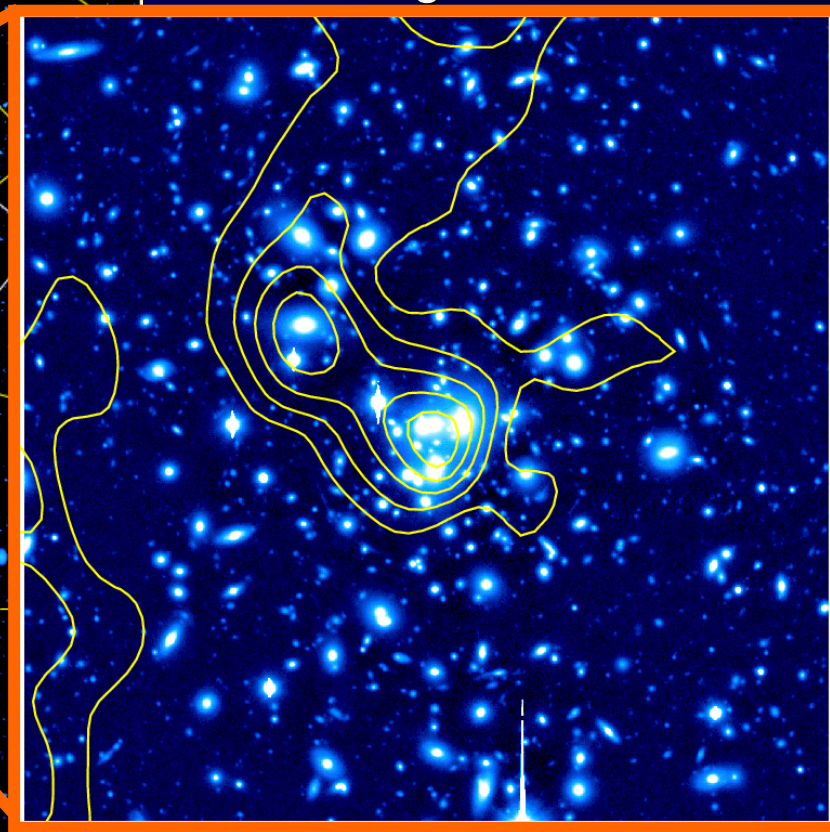

Flexion reconstruction in a 4'x4' region (Okura, Umetsu, & Futamase 2007ab)

Full 2D-based Mass Profile in A1689

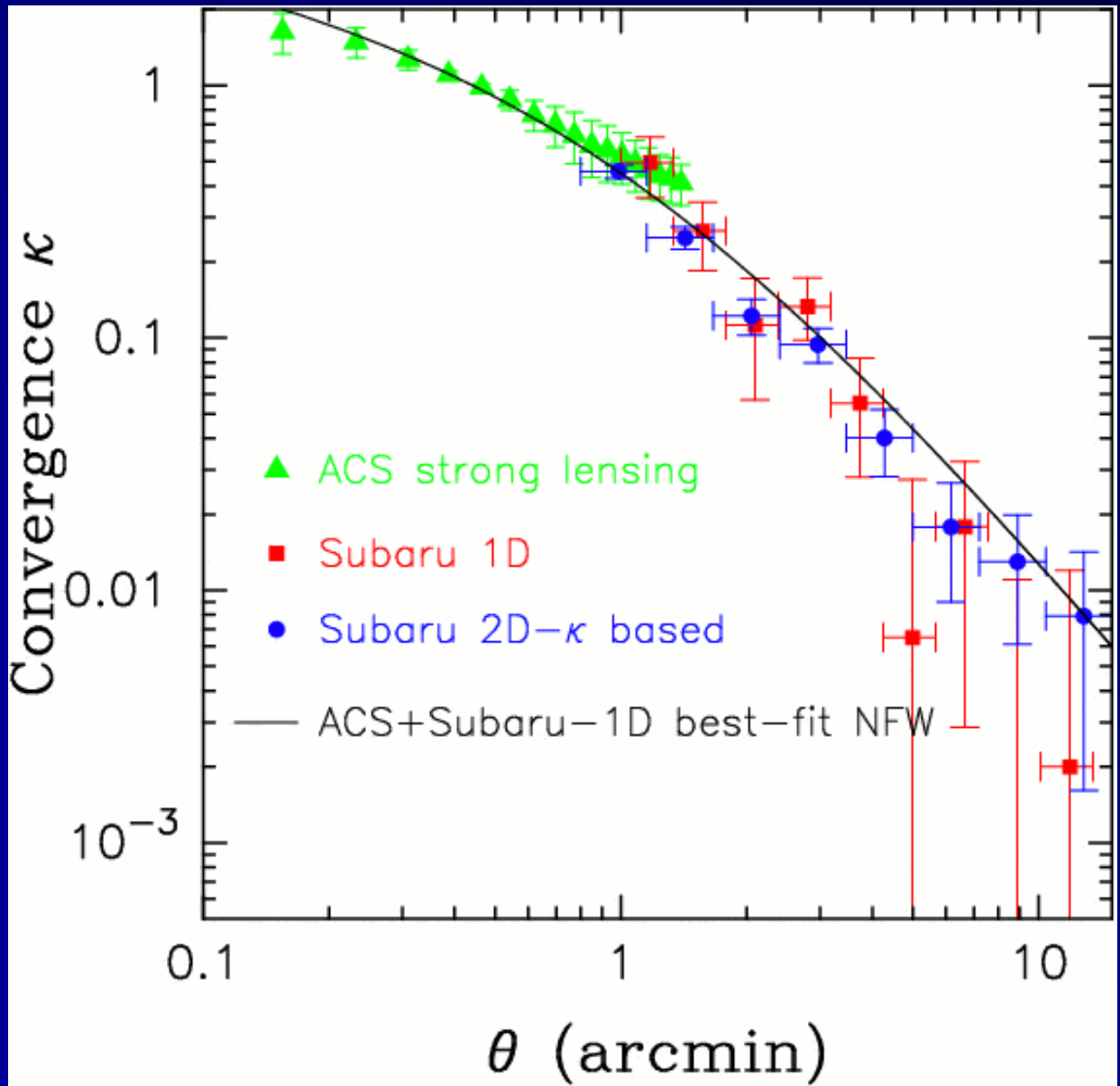

2D-based mass profile (blue) obtained by a 1D projection of MEM reconstructed mass map of A1689

Error bars are correlated

1D and 2D reconstructions are consistent with each other, supporting the assumed quasi circular symmetry in projected mass distribution

UTB2007

Distributions of Mass and Baryons

Subaru/S-Cam R-band image

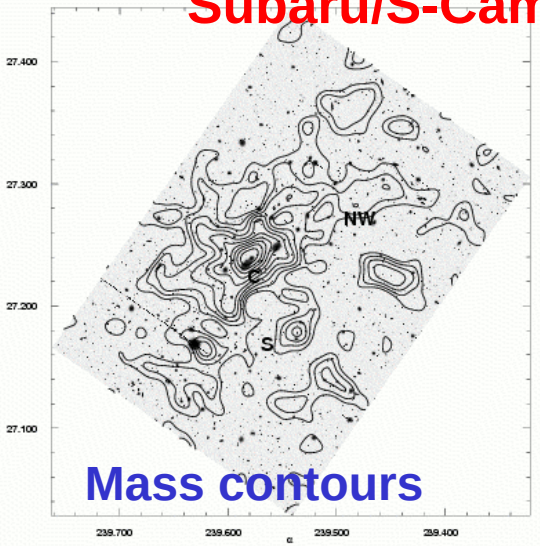

Mass contours

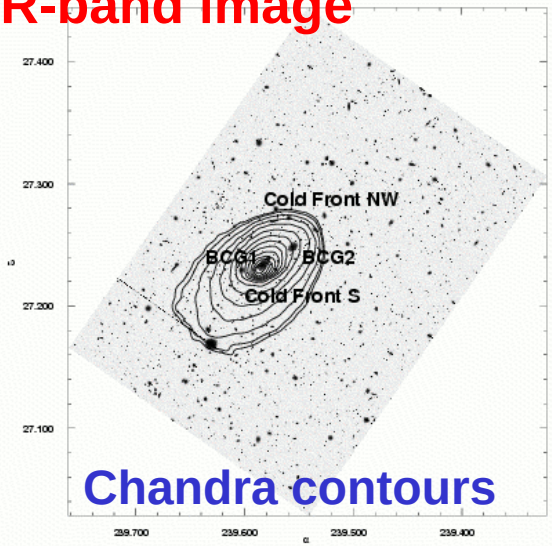

Chandra contours

R-band luminosity

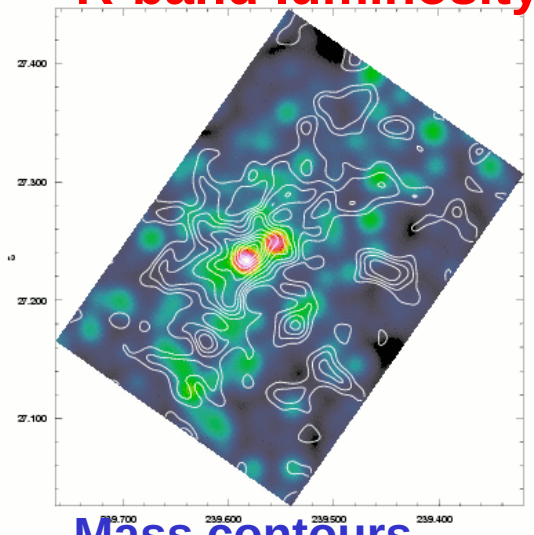

Mass contours

Chandra image

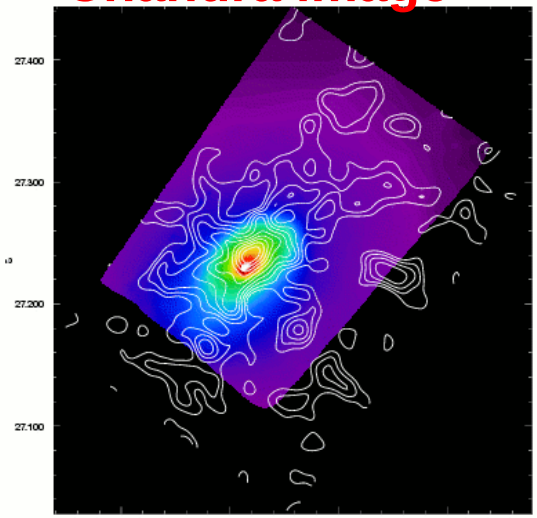

Mass contours

Okabe & Umetsu (2007, PASJ accepted)

Systematic study of 7 nearby merging clusters based on Subaru/S-Cam observations

AMiBA T-SZE

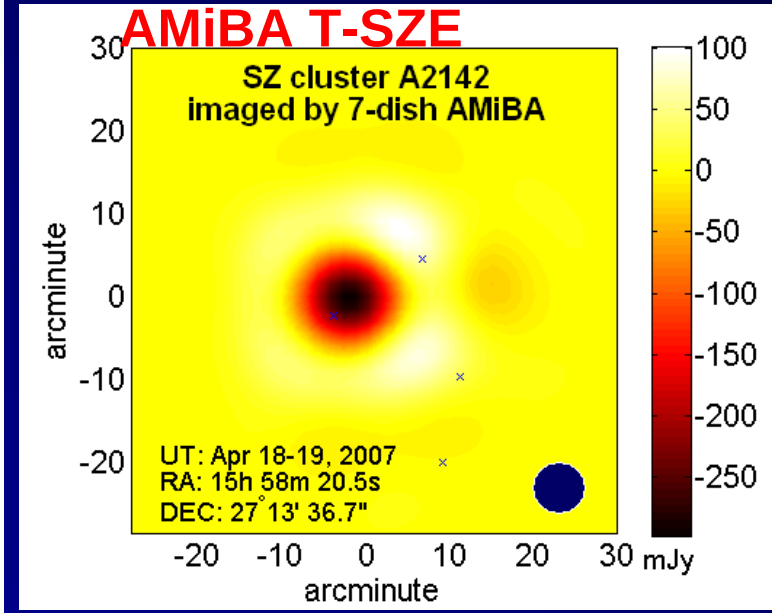

AMiBA team

Summary

- Weak lensing has become a reliable observational tool (not just a theoretical tool) in the past decade thanks to successful developments in practical observational techniques (KSB/IMCAT, Shapelets etc.) as well as in instrumental technology (Subaru, HST, CFHT etc.).

- Cluster weak lensing is now a very hot research topic:

- Mass distributions in merging clusters:: cluster physics, dark matter nature

- Dark matter distributions out to cluster virial radii (or to filaments)

- Strong + Weak lensing to probe the entire mass profile, constraining the nature of dark matter

- The dilution effect by cluster contamination is significant in the cluster central region, leading to systematic underestimations of NFW concentration and virial mass parameters. A secure background selection with color/photo-z information is crucial for cluster mass measurements.

- Thanks to high image quality, Subaru observations allow mass-substructure mapping in z=0.05-0.2 clusters (see also Okura, Umetsu, Futamase 2007ab for the use of the higher-order WL effect, Flexion)

FIN

2.1. Cosmological weak lensing

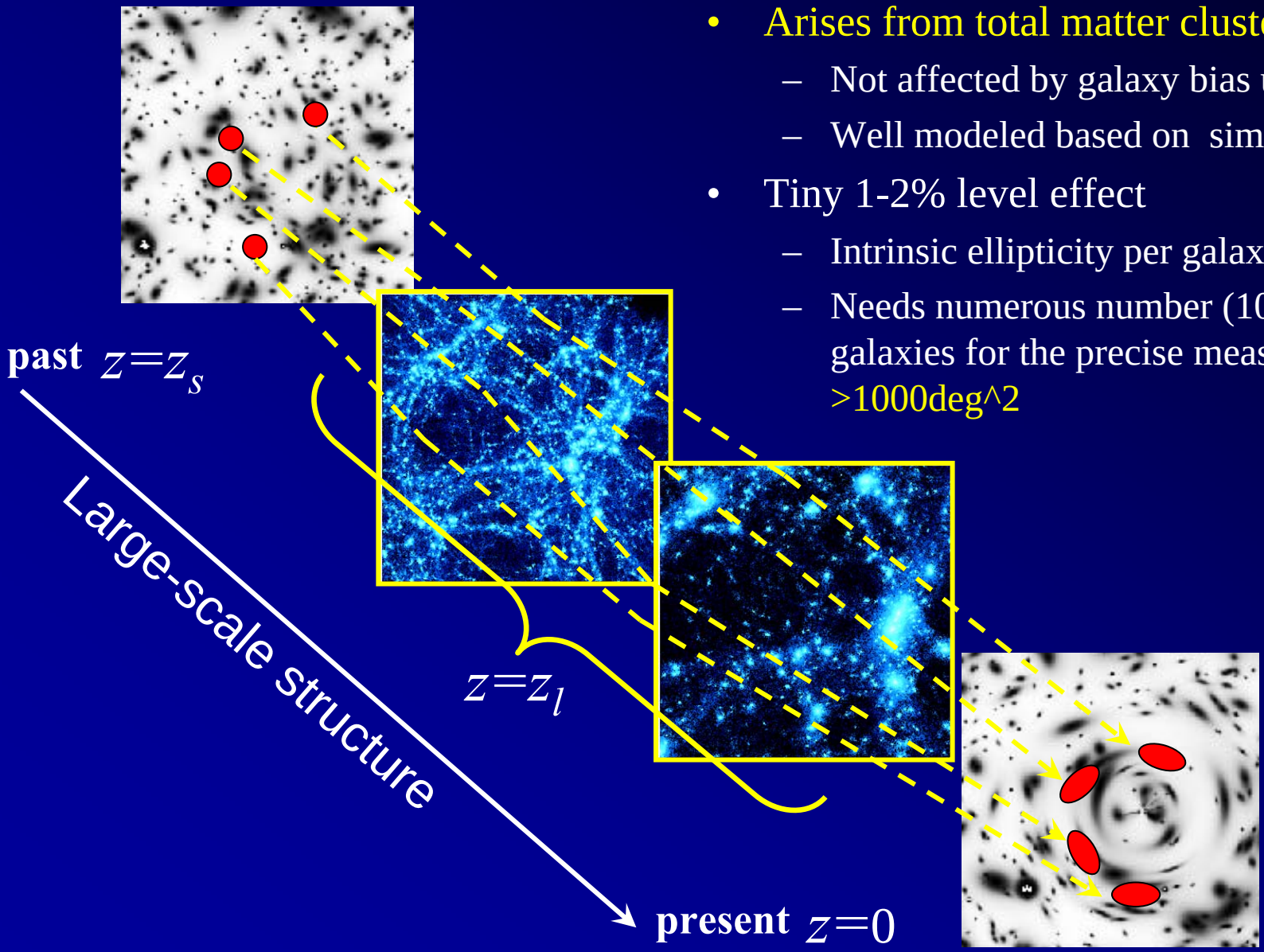

- Arises from total matter clustering
  - Not affected by galaxy bias uncertainty
  - Well modeled based on simulation
- Tiny 1-2% level effect
  - Intrinsic ellipticity per galaxy, ~30%
  - Needs numerous number (10^8) of galaxies for the precise measurement ➔ >1000deg^2

Subaru/Suprime-Cam and Weak Lensing

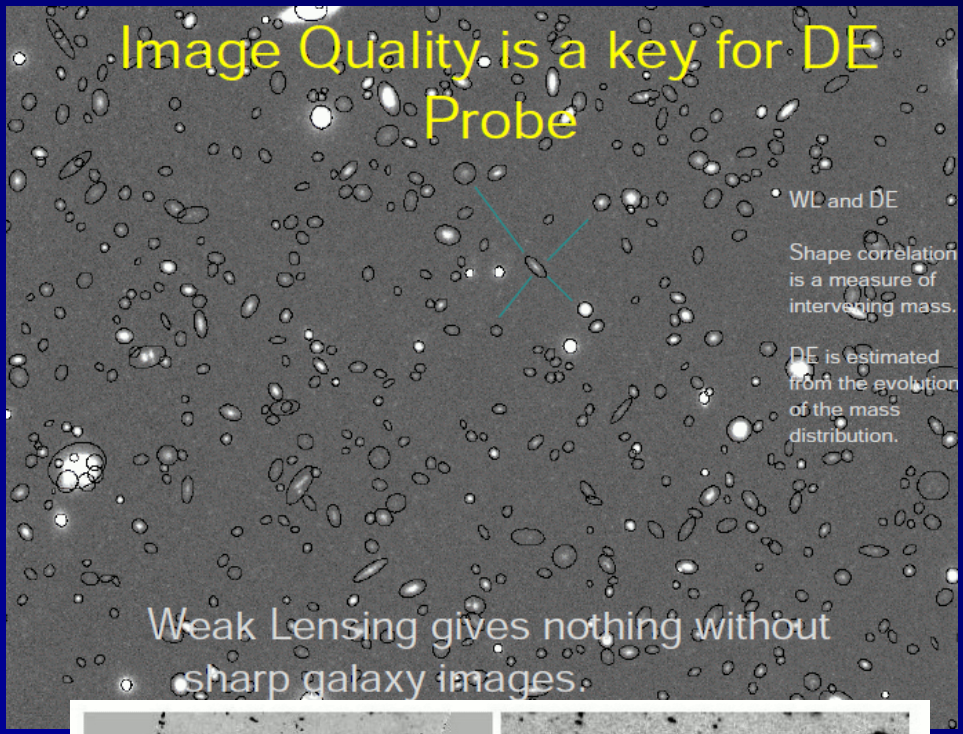

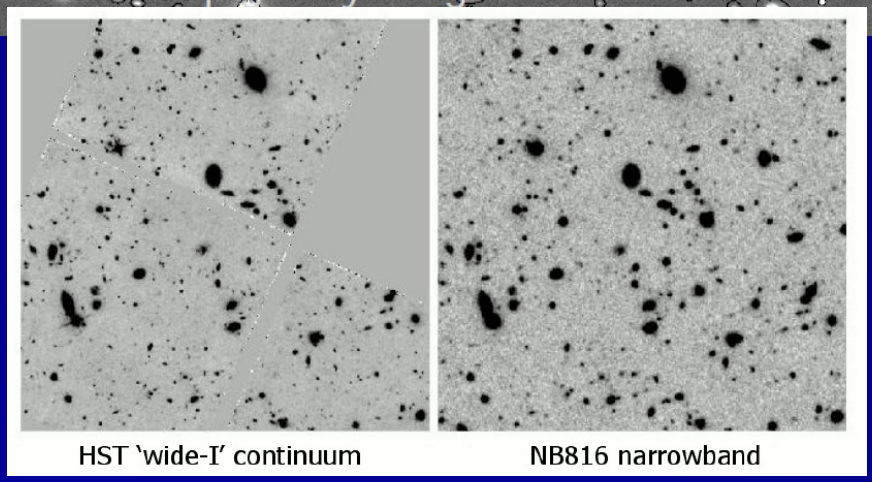

Hu & Cowie 2006 Nature

- Large photon collecting area, D=8.3m
- Wide ~30' x 30' FoV
- Small, stable PSF anisotropy; sub-arcsec seeing
- Ideal instrument for weak lensing (large AΩ and high image quality)

HST and Subaru Telescope

- D=2.4m
- Superb angular resolution
- ~ 3’ x 3’ Field-of-View (FoV)
- Ideal instrument for **strong lensing** in the innermost region

- Large photon collecting area, D=8.3m
- Wide ~30’ x 30’ FoV
- Small, stable PSF anisotropy; sub-arcsec seeing
- Ideal instrument for **weak lensing**, detectable out to virial radii

Validity of weak-field approximation

Validity of the weak-lensing approximation in a cosmological situation?

$$|\Phi|/c^2 \ll 1$$

Poisson Eq.

$$\Delta\Phi = 4\pi G a^2 \bar{\rho}\delta = \frac{3}{2} H_0{}^2 \Omega_m \frac{\delta}{a}$$

$$\frac{|\Phi|}{c^2} \sim \frac{3}{2}\left(\frac{H_0}{c}\right)^2 \lambda^2 \Omega_m \frac{\delta}{a} = \frac{3}{2}\left(\frac{\lambda}{\lambda_H}\right)^2 \Omega_m \frac{\delta}{a}$$

$$\approx 5\times 10^{-6}\left(\frac{\lambda}{10\mathrm{Mpc}/h}\right)^2 \left(\frac{\Omega_m}{0.3}\right)\left(\frac{\delta_0}{1}\right)$$

The potential field can be smooth and small even if the underlying density perturbations are peaky and non-linear

Shape Deformation

$$\delta\beta_i = D_{ij}^{(1)}\delta\theta_j + \frac{1}{2}D_{ijk}^{(2)}\delta\theta_j\delta\theta_k + \ldots$$

$$D_{ij}^{(1)} = A_{ij} = \delta_{ij} - \partial_i\partial_j\psi$$

$$D_{ijk}^{(2)} = A_{ij,k} = -\partial_i\partial_j\partial_k\psi$$

Jacobian matrix (1st order)

2nd order size-dependent deformation [angle^-1], called Flexion (e.g., Okura, Umetsu, Futamase 2007ab)

Deformation matrix modified including higher-order terms, corresponding to highly stretched arcs etc.

$$\frac{\delta\beta_i}{\delta\theta_j} = D_{ij}^{(1)} + D_{ijk}^{(2)}\delta\theta_k + \ldots$$

(Appendix) Multiple Lensing

Lens-equation with (discretized) multiple-lens approximation

$$\boldsymbol{\theta}^{(n)} \approx \boldsymbol{\theta}^{(1)} - \frac{2}{c^2}\sum_{p=1}^{n-1}\Delta\chi_p \frac{r(\chi_n-\chi_p)}{r(\chi_n)}\nabla_\perp \Phi(\boldsymbol{\chi}_p)$$

$$\approx \boldsymbol{\theta}^{(1)} - \frac{2}{c^2}\sum_{p=1}^{n-1}\frac{r(\chi_n-\chi_p)}{r(\chi_n)}\nabla_\perp \psi_p$$

$$\psi_p \equiv \int_{\chi_p}^{\chi_p+\Delta\chi} d\chi_{//}\Phi(\chi_{//},\boldsymbol{\chi}_\perp)$$

Jacobian matrix of lensing:

$$\mathbf{A}^{(n)} \equiv \frac{\partial\boldsymbol{\theta}^{(n)}}{\partial\boldsymbol{\theta}^{(1)}} = \mathbf{I}_{ij} - \sum_{p=1}^{n-1} g(\chi_p,\chi_n)\mathbf{H}_p\mathbf{A}_p \equiv \mathbf{I} - \boldsymbol{\Psi}^{(n)}$$

$$H_{p,ij} = \frac{\partial^2\psi_p}{\partial\chi^i\partial\chi^j}$$

$$\mathbf{A}^{(n)} = \mathbf{I} - \sum_p \Psi_p + \sum_{p,p'}\Psi_p\Psi_{p'} - \sum\Psi_p\Psi_{p'}\Psi_{p''} + \ldots$$

$$= \begin{pmatrix} 1-\kappa-\gamma_1 & -\gamma_2-\omega \\ -\gamma_2+\omega & 1-\kappa+\gamma_1 \end{pmatrix}$$

(Appendix) Cumulative Mass Estimator

Aperture densitometry, or so-called z-statistic mass estimator (Fahlmann et al. 1994; Clowe et al. 2000), in terms of observable galaxy shear estimates:

$$\zeta(\theta;\theta_{\rm max}) := \frac{2}{1-\theta^2/\theta^2_{\rm max}} \int_\theta^{\theta_{\rm max}} d\ln\vartheta\,\langle\gamma_+(\vartheta)\rangle = \bar{\kappa}(<\theta) - \bar{\kappa}(\theta<\vartheta<\theta_{\rm max})$$

- θ_{max} be taken as large as possible (θ_{max} <~ 15'-20' for Subaru/Scam)
- ζ(R) is measured from outside of R, allowing to avoid the inner strong lensing regime!!!

The following gives a lower bound to the enclosed mass:

$$M(<\theta) > M_\zeta(<\theta) \equiv \pi(D_d\theta)^2\Sigma_{\rm crit}\zeta(\theta;\theta_{\rm max}) = M(\theta) - \pi(D_d\theta)^2\Sigma_{\rm crit}\bar{\kappa}(\theta<\vartheta<\theta_{\rm max})$$

mean background, similar to the concept of background subtraction in photometry

Example: A1689 (Subaru/S-Cam)

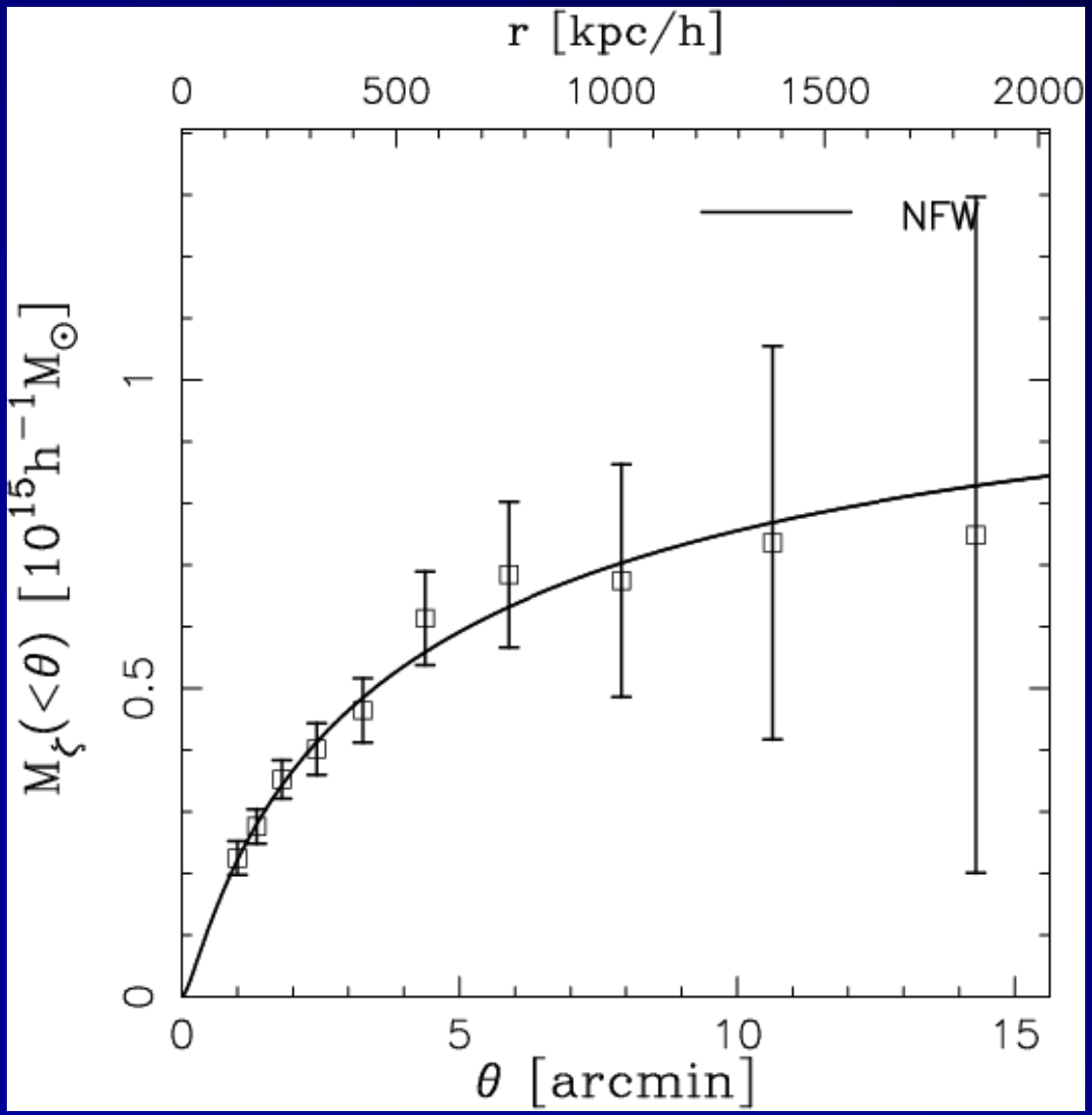

ζ-statistic cumulative mass measurements assuming <zs>=1 for the red-background sample;

θ_{max}=19 arcmin, while the projected virial radius is θ_{vir} ~ 15 arcmin

Note the errorbars are correlated!

Measurement (I): tangential shear

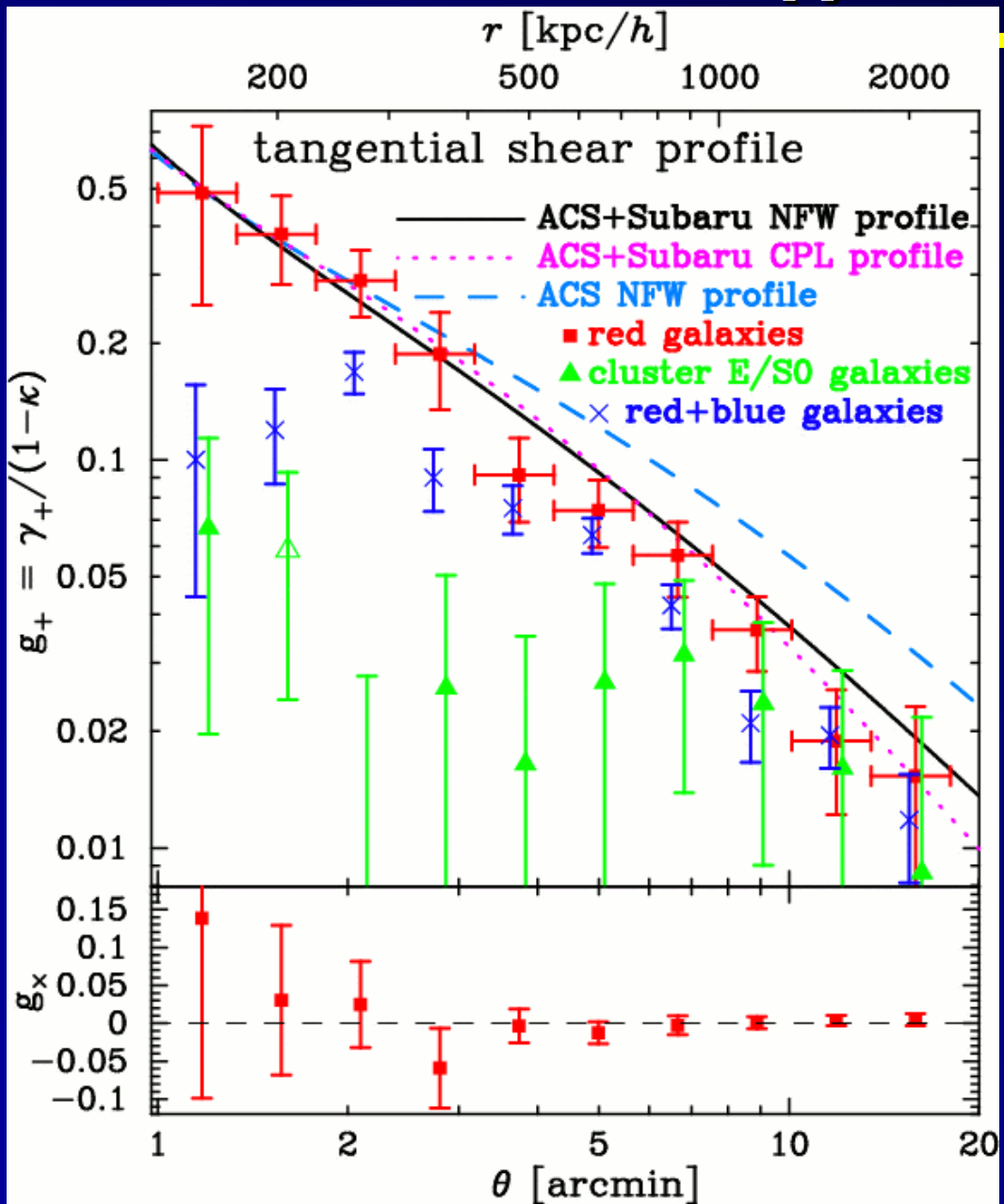

- Significant S/N of 12σ ( )
- Signal being diluted by a factor of 2-5 without a secure background selection (X)
  cf., Clowe & Schneider 2001; Bardeau et al. 2004
- Good agreement with ACS @ r < 3'
- Signal strength @ r > 3' is weaker than expected from ACS
- Null-detection of B-mode signal, $\mathbf{g_x}$ → No significant systematics

Measurement (II): magnification bias

Number counts of the Background

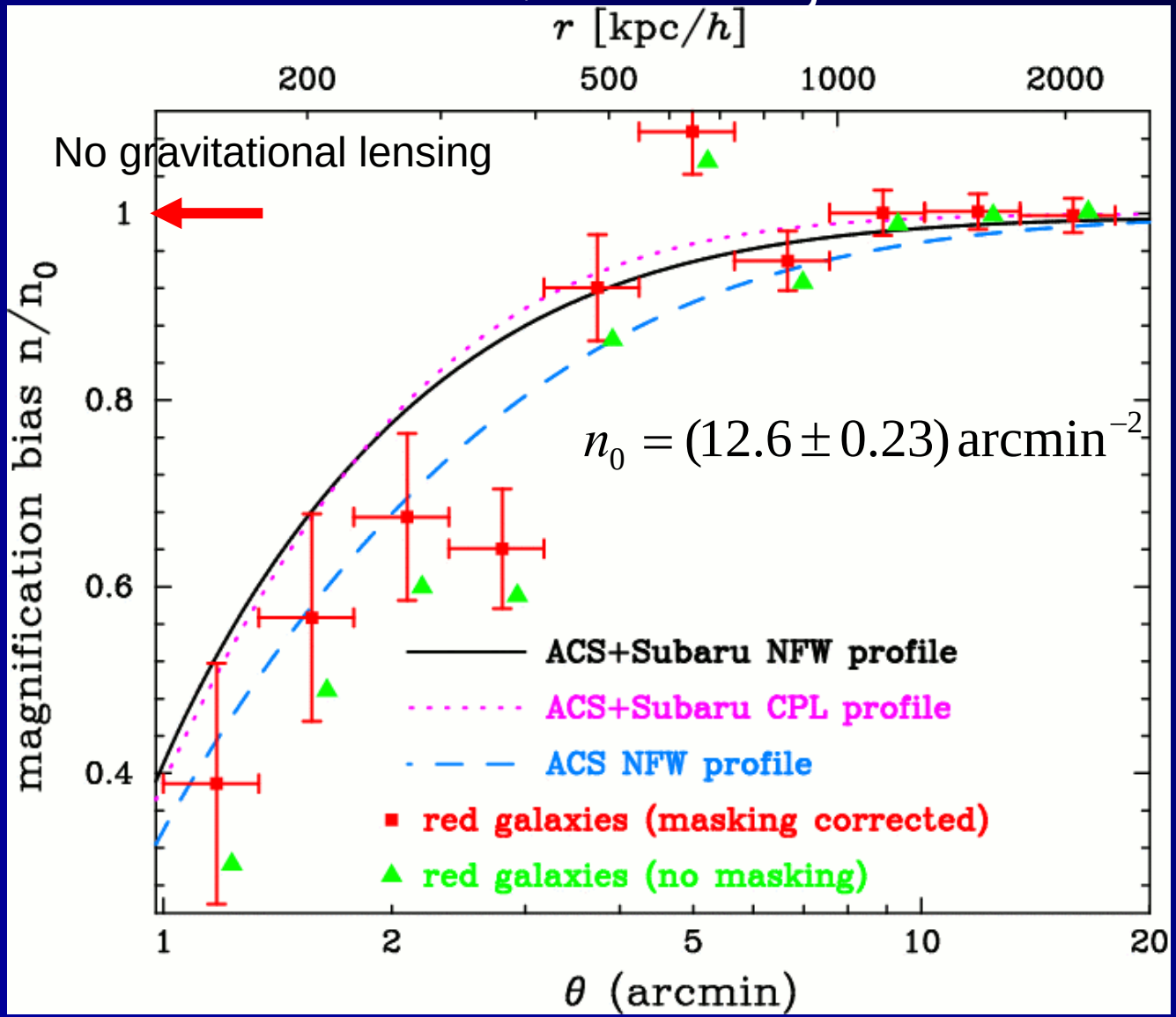

- Significant detection of a **depletion** of red galaxy counts (9.3 σ)
- Signal @ r>3' is weaker than expected from ACS
- Masking effect by member galaxies corrected ( )

Dilution vs. Lensing Magbias Effect

$$\frac{\delta n_g}{n_{g0}} = 1 + \delta_{\rm dilution} + \overset{\rm GL}{\delta_{\rm magbias}}$$

Depression of background # counts due to gravitational magnification bias

$$\delta_{\rm magbias} \approx 2(\alpha - 1)\kappa < 0$$

$$\delta_{\rm magbias} \approx 2(\alpha - 1)\kappa \sim -0.3\left(\frac{\kappa}{0.3}\right) @\ \alpha = 0.2$$

α<1 found at fainter magnitudes of redder optical bands
cf. α~0.22 at i'=25.5 (BTU05)

Contamination by cluster galaxies (dilution of lensing signal)

$$\delta_{\rm dilution} = \frac{n_{\rm cluster}}{n_{g0}}$$

$\delta_{\rm dilution}$ ~ several in the central region of rich clusters

Weak Lensing Halo Surveys

Schneider 1996, Erben et al. 2000, Umetsu & Futamase 2000, Miyazaki et al. 2003 etc..

On-going/Future surveys: CFHTLS, GaBoDS, / Pan-STARRS, Subaru HSC etc..

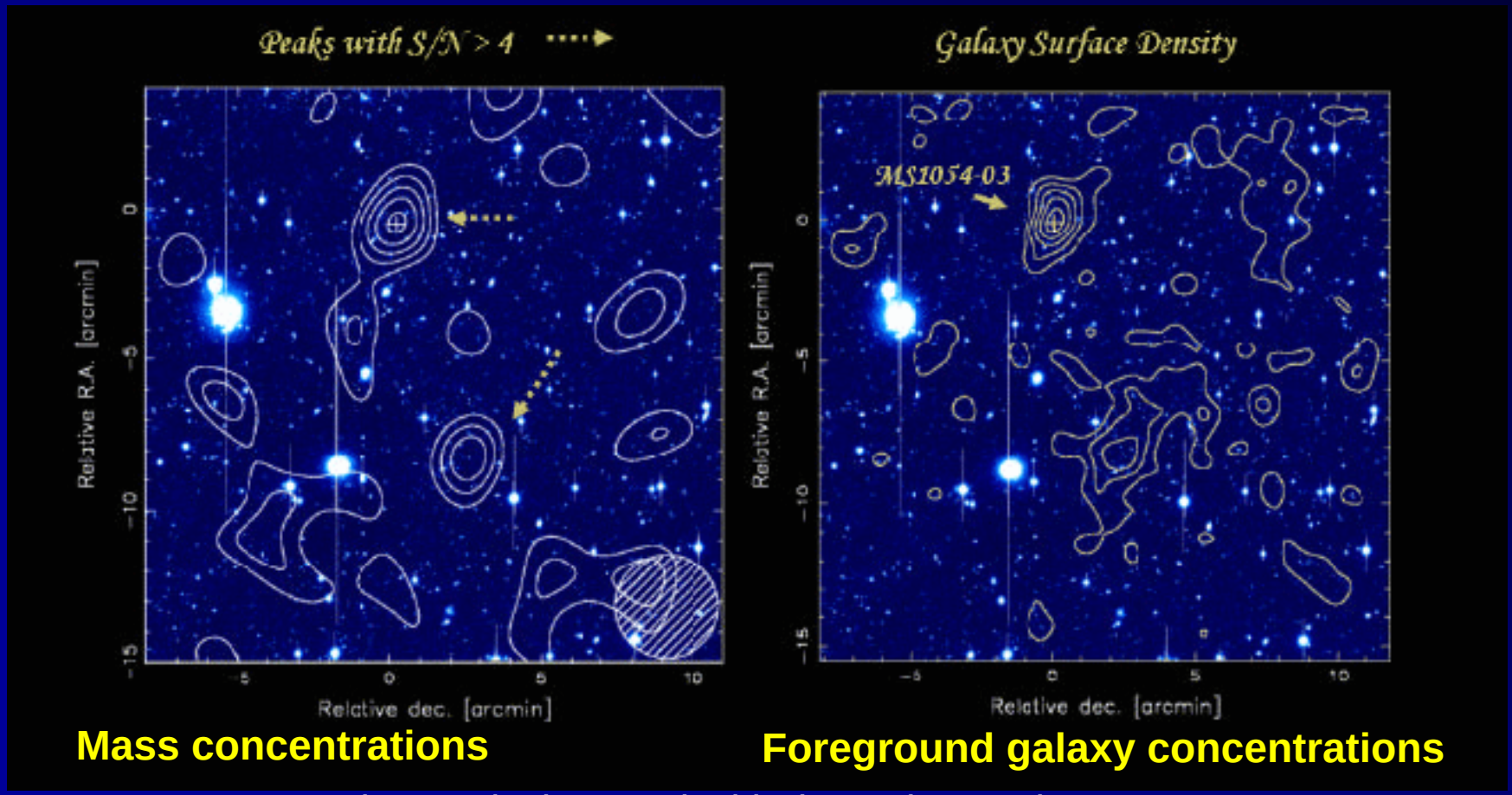

Mass concentrations **Foreground galaxy concentrations**

MS1054-03 (z=0.83) observed with the Subaru telescope